UNIVERSITY OF CALIFORNIA
Santa Barbara

Indium-Phosphide Based Narrow-Band Optical Filters and Add-Drop Multiplexers

by

Thomas Liljeberg

A dissertation submitted in partial satisfaction of the requirements for the degree of

Doctor of Philosophy
in
Electrical and Computer Engineering

Committee in charge:

Professor John E. Bower, Chairperson
Professor Daniel J. Blumenthal
Professor Larry A. Coldren
Professor Nadir Dagli

June, 2002

The dissertation of Thomas Liljeberg is approved

Professor Daniel J. Blumenthal

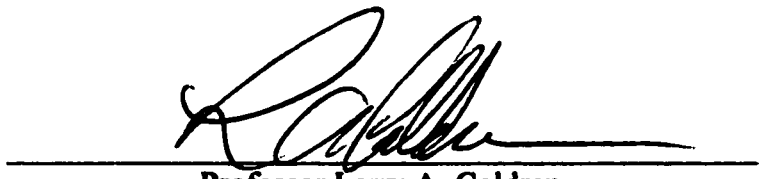

Professor Larry A. Coldren

Professor Nadir Dagli

Professor John E. Bowers, Chairperson

June 2002

Indium-Phosphide Based Narrow-Band Optical Filters and Add-Drop Multiplexers

Acknowledgements

Looking back at my time in graduate school at UCSB, I feel incredibly fortunate for the opportunity to learn from and work with professors and researchers at the very top of their field. The people who deserve thanks and acknowledgements are far too numerous to list here, however, this dissertation would not be complete without specifically mentioning a few people.

First and foremost, I want to thank my advisor, Professor John Bowers, for his support through my years in his research group, and for the advice, direction, creativity and enthusiasm he was a constant source of. I also wish to thank my committee, Professors Blumenthal, Coldren and Dagli for their advice and input, and for asking the right questions.

Kehl Sink also deserves acknowledgements here. Besides being a good friend, he was always great to bounce good – and not so good – ideas off.

Dubravko Babic gave me a good start in the clean room, and showed me where to get coffee at 3 am, both essential for the years of graduate school to follow. Also thanks to Alexis Black and Volkan Kaman for many good conversations, research related and other. Thanks to Patrick Abraham for advice and epi.

Naturally, a world exists outside the University and outside the lab. Jee-Yeon Ryu reminded me of that, and I will always be grateful for her support and friendship.

Finally, I wish to dedicate this work to my parents, Leif and Ingrid Liljeberg. They taught me to have high personal standards and expectations for myself. From I was quite young, they trusted me and gave me the freedom to make my own decisions and learn to navigate for myself; their love and support provided the safety net that made it possible me for to take advantage of that freedom.

Vita of Thomas Liljeberg

November 25, 1969	Born in Copenhagen, Denmark
August 1993	Cand. Polyt. (M.S. Electrical Engineering) Specialization: Communication Systems, Information Theory Technical University of Denmark
September 1993-October 2000	Research Assistant Dept. of Electrical and Computer Engineering, University of California, Santa Barbara Santa Barbara, California
June 1995	M.S. Electrical Engineering University of California, Santa Barbara Santa Barbara, California
June 2002	Ph.D. Electrical Engineering University of California, Santa Barbara Santa Barbara, California

Publications

Journal papers and conference presentations

Liljeberg, T., Tohmon, R., Hall, E., Abraham, P., Focht, M., Fish, G.A., Larson, M.C., and Coldren, L.A., "High-Power, Widely-Tunable Sampled Grating DBR Laser Integrated with a Semiconductor Optical Amplifier", *accepted for presentation at the 18th International Semiconductor Laser Conference, Garmisch, Germany, October 2002*

Akulova, Y.A., Fish, G.A., Schow, C., Larson, M., Liljeberg, T., Karim, A., Hall, E., Wipiejewski, T., Pavinski, D., Butrie, T., and Coldren, L., "Widely-Tunable Electroabsorption-Modulated Sampled Grating DBR Laser", *LEOS 2001, 14th Annual Meeting of the IEEE Lasers and Electro-Optics Society, San Diego, CA, 2001*

Liljeberg, T., and J.E. Bowers, "Design and modeling of InP waveguide based narrowband optical filters and Add-Drop Multiplexers for WDM applications", *Proceedings of SPIE, vol. 4283, SPIE Optoelectronics 2001 Conference/Physics and Simulation of Optoelectronic Devices IX (Physics and Simulation of Optoelectroni Devices), San Jose, CA, 2001*

Kaman, V., Y.-J. Chiu, T. Liljeberg, S.Z. Zhang, and J.E. Bowers, "A compact 40 Gbit/s receiver based on integrated tandem electroabsorption modulators", *Electron. Lett., vol.36, no.23, p.1943-4, Nov. 2000*

Kaman, V., Y.-J. Chiu, T. Liljeberg, S.Z. Zhang, and J.E. Bowers, "Integrated Tandem Traveling-Wave Electroabsorption Modulators for > 100 Gbit/s OTDM Applications", *IEEE Photon. Technol. Lett., vol.12, no.11, p.1471-3,Nov. 2000*

Kaman, V., Y.-J. Chiu, T. Liljeberg, J.E. Bowers, and S.Z. Zhang, "Integrated tandem electroabsorption modulators for high-speed OTDM applications", *International Topical Meeting on Microwave Photonics MWP 2000, Oxford, UK, 2000*

Liljeberg, T., and J.E. Bowers, "Velocity mismatch limits in semiconductor lasers and amplifiers", *paper TuY6, pp. 341-2 in Conference Proceedings, LEOS '97, 10th Annual Meeting, IEEE Lasers and Electro-Optics Society 1997.*

Other publications

Liljeberg, T. and J.E. Bowers, "High-Speed Semiconductor Lasers and Photodetectors", in "Electro-Optics Handbook", 2nd ed., R.W. Waynant and M. Ediger (eds.), McGraw-Hill, April 2000, ISBN 0070687161

Abstract

Indium-Phosphide Based Narrow-Band Optical Filters and Add-Drop Multiplexers

by

Thomas Liljeberg

Reconfigurable, narrowband optical filters and add-drop multiplexers (ADMs) are key components for versatile high-capacity fiber-optic wavelength division multiplexed (WDM) communication systems. Implementing the filters and ADMs in semiconductor waveguide technology opens possibilities for integration with other passive and active devices for high-functionality modules.

The dissertation describes design, fabrication and characterization of InP waveguide based filters and ADMs with optical bandwidths below 50 GHz.

The devices are based on distributed Bragg reflector (DBR) filters. Methods to achieve optical bandwidths sufficiently narrow for dense-WDM are discussed. By using quarter-wave shifted DBR gratings in low loss waveguides, optical filter bandwidths of 38 GHz at 1.55μm wavelength were demonstrated. The bandwidth of these first-order filters was limited by waveguide propagation loss; design approaches for implementation of higher-order filters with even smaller bandwidth and less sensitivity to losses will be discussed. Finally, the dissertation covers integration of the narrowband filters with directional couplers to obtain add-drop multiplexers.

Contents

Chapter 1 Introduction

1.1 Introduction

Over the past decade, a revolution has taken place in the area of data and telecom communication systems and networks. Only 10 or 15 years ago, the vast majority of the information transmitted on large networks was "plain old telephony", that is, voice transmitted on circuit switched networks. Today, the picture is dominated by data transmission over high capacity packet switched networks. With the explosion in Internet and World Wide Web use, and introduction of new services and applications, demand for data transmission bandwidth has grown at astronomical rates. Some of the factors driving this growth are the increasing number of people with Internet access, along with a number of new and more bandwidth demanding applications and services. Finally, more and more companies are deploying high capacity intranets and extranets to share information between employees, and between company and customers or suppliers. While the growth in number of people connected to the Internet is slowing down, particularly in the US and Western Europe, the information accessed continues to be more and more bandwidth demanding, e.g. pictures and video. Combined with the growth from new services and new ways to access the networks, this promises to maintain a very high growth rate in the bandwidth demand, see projection in Figure 1.1.

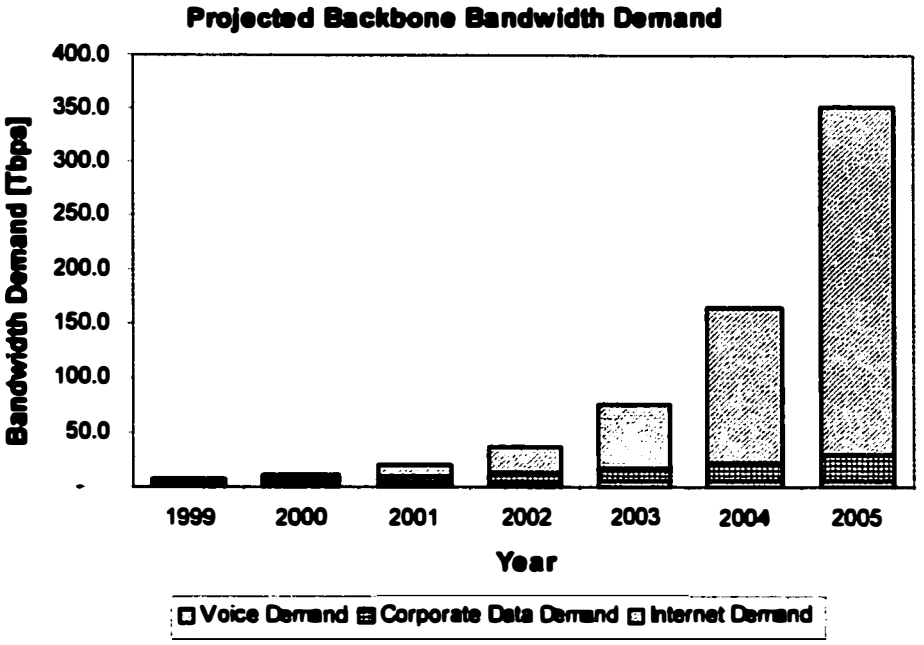

***Figure 1.1** Projected bandwidth demand (March 2001 projection).*

At the same time, new technologies (along with deregulation and increased competition) have significantly contributed to bringing down the cost of bandwidth. This cost reduction has fueled the innovation of new services, which in turn has provided the incentive to further increase bandwidth and decrease cost. While this virtuous cycle has slowed down somewhat in the recent year, the long-term projections continue to predict a very high growth rate in bandwidth demand, pushing the development of technologies capable of supplying faster, cheaper and more versatile networks

1.2 WDM Networks

Several technologies co-exist and compete to provide the increased bandwidth. As mentioned, a shift has taken place from circuit switched to packet switched networks, providing more flexibility and versatility. Erbium doped fiber amplifiers have dramatically increased the distance data can be transmitted without costly electronic regeneration. Increasingly faster electronics has pushed the limit for maximum bandwidth achievable with electronic time-division multiplexing (TDM). 40 Gbit/s TDM systems are now commercially available, and even higher single-channel bit rates can be achieved with optical time-division multiplexing (OTDM). Systems with single channel bandwidth of over 160 Gbit/s have been demonstrated in research laboratories.

The advent of wavelength division multiplexed (WDM) systems has made it possible to dramatically increase the transmission bandwidth of both existing fiber links and new systems; systems with a potential aggregate bandwidth of over 1 Tbit/s are now available.

One advantage of WDM systems is the possibility of routing and processing on the optical level, instead of detecting and processing in the electrical domain before re-transmitting the optical signal. Wavelength routed passive networks is a relatively simple example of this; the trend is towards doing more and more of the routing and switching in the optical domain.

Some of the key components for optical routing and switching are wavelength multiplexers and demultiplexers, all-optical cross-connects and switches, and Add-Drop multiplexers (ADMs). Currently most of switching, routing and cross-connect functions are performed in the electrical domain, requiring complex and expensive high-speed electronics. By moving as much as possible of this processing to the optical domain, smaller complexity can be achieved, in addition to greater transparency with respect to modulation speed and format.

1.3 Add-Drop Multiplexers

Add-drop multiplexers are key components for high capacity packet switched optical networks. The basic functionality of an ADM is illustrated in Figure 1.2.

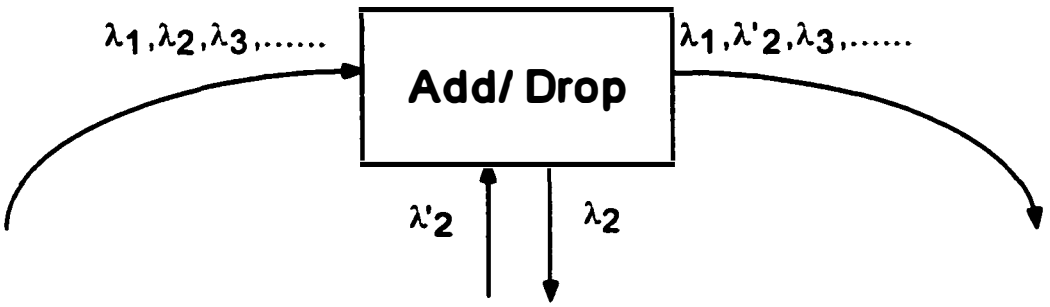

***Figure 1.2** Add-Drop Multiplexer*

All the channels are incident on the *in* port, and the ADM selectively picks out one channel, which is dropped and processed, and new data is inserted on that channel and transmitted. Ideally, the device is completely transparent, not only to data on

the other channels, but also to coding and modulation formats of the dropped channel.

The benefits from all-optical add-drop functionality depend on the network structure. Smaller networks, such as local area networks, campus/enterprise networks and metro area networks are typically implemented using simple broadcast ring or bus topologies. In these types of networks, the main benefit of an all-optical ADM is a reduction in complexity and processing. A node can be statically or quasi-statically assigned a specific wavelength channel, leaving all the routing and processing to take place at a central hub. This approach keeps the components at the each node as simple as possible, and thereby cheap. Added network flexibility and total capacity can be increased at the cost of higher complexity and price, by using dynamically reconfigurable ADMs at the nodes.

In larger networks, i.e. long-haul networks or WANs, the network is based on a mesh-structure. The nodes can have different levels of complexity, ranging from complex sub-systems with demultiplexers, cross-connects, multiplexers, and possible wavelength converters, to simpler nodes based on add-drop multiplexers.

In the past, connections were established based on circuit switched protocols, i.e. when a connection is established, a permanent path through the network, between the two endpoints is established for the duration of the connection. Newer fiber-optic networks are based on packet switching, but on the electrical/logical level. On the physical/optical level, connections between two nodes in the network are still established semi-permanently. A true packet switched network would have

greater flexibility and reliability, but also place much higher requirements on the components. To achieve packet switching on the optical level, fast switches and ADMs capable of being reconfigured at packet rate, are needed.

The remainder of this section reviews the technologies available to implement all-optical add-drop multiplexers, and compares the performance on different parameters, such as cross-talk, reconfigurability, speed, and optical bandwidth.

Referring back to Figure 1.2, they basic functionality of an ADM is spatial separation of one wavelength channel from all other channels. The conceptually simplest way of achieving this is using a reflection filter in conjunction with two optical circulators, as shown in Figure 1.3.

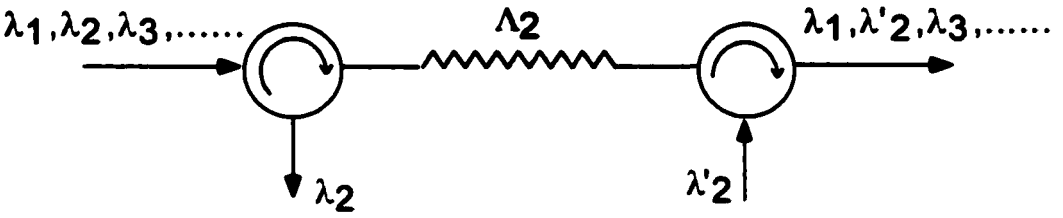

***Figure 1.3** Simple example of an Add-Drop Multiplexer based on a DBR-filter and two optical circulators.*

N wavelength channels are incident on port 1 and pass through the circulator to the filter, where all the out-of-band channels are transmitted and passed through the second circulator to the output. The on-resonance channel is reflected, and sent to the drop port by the circulator. Similarly, the signal applied to the add port goes

through the circulator, is reflected by the filter and then sent to the output port by the circulator. Devices based on this structure were the first to be demonstrated in laboratories. The filter can be based on one of several technologies; the most commonly demonstrated employ a fiber grating filter, but waveguide filters have also been used. Because the circulators have very low transmission from port 1 to port 3, the performance of the ADM is essentially limited by the filter characteristics.

In terms of actual system deployment, the concept shown in Figure 1.3 is not advantageous – circulators are expensive, and alignment and packaging further add to the cost. Currently, commercially available ADMs are typically based on Silica on Si arrayed waveguide gratings (AWGs) [1-7]. These ADM devices are really integrated devices consisting of demultiplexers, 2x2 switches and multiplexers. An example with 16 channels is shown in Figure 1.4.[1].

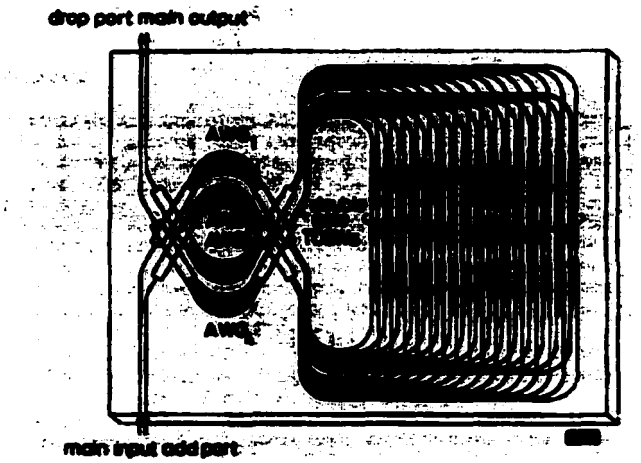

Figure 1.4. *Silica-on-Si 16-channel Add-Drop Multiplexer based on Arrayed Waveguide Gratings and thermo-optic 2x2 switches [1].*

The device is connected to the network at port 1 and the add channels are applied to port 2. The first AWG demultiplexes both the signal from the network and the local add signal. Note that this allows for simultaneous add-drop operation on any number of channels; port 2 can be a single channel or a local tributary input or subnet. The 2x2 switches are thermo-optic switches, limiting the maximum switching speed to the μs-range. After the switches, all the channels are multiplexed again, and appear on the two output ports.

The limits to the performance of these devices are determined as follows: For speed, the switching speed of the 2x2 thermo-optic switches limits reconfiguration speed to the MHz range at the very best. Total channel count is limited by the bandwidth and the free spectral range of the AWG; the potential for over 300 channels has been demonstrated in research labs [5]. The channel spacing is limited by the static filter characteristics of the AWG, which is theoretically limited by the number of waveguides in the array, and practically by control over material, process and temperature. Devices with 10 GHz channel spacing and better than 20 dB cross-talk isolation have been demonstrated [8]. Based on Silica-on-Si technology, the device is not readily integratable with semiconductor based active devices, although some work has been done with hybrid integration and with semiconductor AWGs [9].

Another technology for implementing ADMs is semiconductor, dielectric or fiber-based cascaded Mach-Zehnder interferometers [10-12], as illustrated in Figure 1.5, which shows an implementation in dielectric waveguides. The approach is based

on resonant couplers, with the phase shift and coupling in the individual sections adjusted to achieve the desired transmission characteristics. Tuning is achieved by separate heating of the stages, limiting the switching speed to the sub-ms range. Control of temperature is also used to compensate for phase-errors in the arms of the interferometers due to fabrication tolerances. The example shown in Figure 1.5 is designed for a channel spacing of 200 GHz and has a cross-talk isolation of better than 20dB. ADMs with channel spacing of 100 GHz have also been demonstrated.

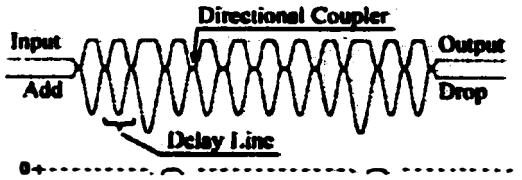

Figure 1.5. *16-channel resonant Mach-Zehnder Interoferometric Add-Drop Multiplexer with 200 GHz channel spacing [10].*

The response of the cascaded MZ-interferometers is periodic, limiting the total number of channels to the free spectral range (FSR) of the device. FSR is determined by the phase difference between the arms in the interferometers, whereas the total number of stages determines finesse, and thereby optical bandwidth and channel spacing. These parameters set a practical limit to the channel spacing and the total number of channels. The best results from research

laboratories demonstrate add-drop operation on one of 16 channels in a 100 GHz system, with 20 dB isolation.

The wavelength and spatial separation of channels can also be achieved with an acousto-optic tunable filter (AOTF)[13-19], illustrated in Figure 1.6.

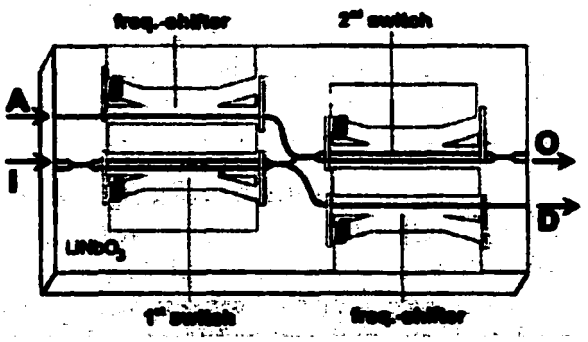

Figure 1.6. *Two-stage acousto-optic tunable filter ADM [13].*

The principle of the AOTF can be described as follows: The acoustic wave creates a traveling- or standing-wave index perturbation in the acousto-optic material. This wave pattern acts as a DBR filter with the resonance condition:

$$\lambda = 2\Lambda \sin(\theta_B)$$

where λ is the optical wavelength, Λ is the wavelength of the acoustical wave and θ is the angle of incidence. For a given angle of incidence, the reflected wavelength can be determined by controlling the wavelength of the acoustic wave, i.e. the frequency of the acoustic signal determines which wavelength(s) the device reflects. By exciting the device with more than one frequency, several channels

can be sent to the drop port, although this causes degradation in the cross-talk isolation, due to non-linear interaction between the frequency components of the acoustic signal.

The ADM performance of an acousto-optic filter is limited by several factors. The minimum switching time is determined by the width of the incident beam; for telecom applications the AOTF are typically based on $LiNbO_3$ and have switching times in the 10-100μs range. The cross-talk isolation can ideally be arbitrarily good by increasing the power of the acoustic signal and using material with high photoelastic coefficient. The device shown in Figure 1.6 has a filter bandwidth of 2 nm, and a cross-talk isolation of 30 dB, on par with state-of-the-art in published literature.

Recently, add-drop filters based on coupled microring resonators in SiO_2 on Si have been demonstrated [20-23]. The filters are based on ring waveguides coupled to input and output waveguides in a regular grid. The main advantage of this architecture is the compact size. The main disadvantages are the strict requirements on process control and the limited free spectral range of microring resonators.

The last type of ADMs covered in this review is semiconductor waveguide based devices, where the filter effect is obtained with DBR gratings or grating-assisted couplers. The basic concept of these devices is very similar to that of the ADMs

and filters that are covered in this work; for details, the reader is referred to the relevant chapters.

Several groups have worked on semiconductor DBR based filters and ADMs [24-36]. In Figure 1.7 [35], a 4-channel tunable filter is implemented using four DBR gratings with different grating period. The device is polarization-independent and tunable through carrier injection in the waveguide layer. This work is based on a linear waveguide, that is, the filters are not integrated with any form of coupler - for ADM applications external circulators are necessary. The filter bandwidth for each of the filters was ~2nm, the channel cross-talk isolation was better than 18 dB for all four channels.

The same group has also demonstrated a multi-channel tunable filter with integrated amplifier, illustrating the potential for integration in the InP system.

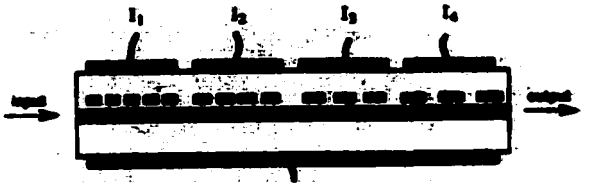

***Figure 1.7** 4-channel Add-Drop Multiplexer implemented as 4 DBR gratings in an InP waveguide. The device is a two-port, requiring external optics to separate incident and reflected waves [35].*

For use as a filter or ADM in a WDM system, the biggest problem with the InP waveguide based technology is achieving a sufficiently narrow drop bandwidth

with a simple DBR filter. The slightly different approach in Figure 1.8. overcomes this problem by using a grating assisted counter-directional coupler [27].

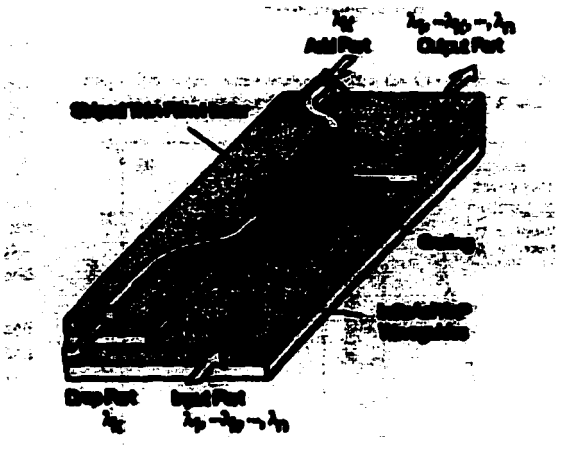

***Figure 1.8** 4-port optical Add-Drop Multiplexer implemented using a grating-assisted counter-propagating directional coupler. The drop bandwidth is 0.4 nm, and the device can be temperature tuned over 11nm [27].*

For InP based ADMs, this represents state-of-the-art. The wavelength selection is achieved using a vertical grating assisted coupler. A drop bandwidth of 0.4 nm (~50 GHz) has been demonstrated with a polarization independent device. The grating is apodized to suppress sidelobes, which cause severe channel cross-talk. With a 100 GHz channel spacing, the measured cross-talk is below 24 dB. In a two channel 2.5 Gbit/s demultiplexing experiment, a bit-error rate penalty of 1.5 dB for the through channel was achieved. The dropped channel experienced no power penalty.

The wavelength is tunable over 11 nm, using an integrated Cr strip heater element. This makes tuning slower, but there is no inherent reason why the same structure could not be implemented using carrier injection (plasma loading) as tuning mechanism, allowing for tuning on nanosecond time scale. The main problem is the increased loss incurred by free-carrier absorption. This limitation will be discussed in detail in a later chapter.

Table 1.1 summarizes this review of ADM technologies. Each of the technologies has specific advantages and disadvantages, and the most suitable approach for a given application depends on the specific requirements.

	Fiber grating	Silica-on-Si AWG	MZI	AOTF	InP – DBR
Filter BW	~ 1nm	<25 GHz (0.2 nm)	~0.7 nm	~ 1.5 nm	~0.4 nm
Cross talk	< -20 dB	< -30 dB	< -18 dB	< -20 dB	<-20 dB
Integration	No	Hybrid	Yes	No	Yes
Scalability	Cascaded	Yes	Cascaded Small #ch	Limited	Cascaded Small #ch
Re-configurability	Temp/Mec (sub-ms)	Temp (sub-ms)	Temp (sub-ms)	Yes (sub-ms)	Temp/ Current

Table 1.1 *Comparison of various ADM technologies.*

The devices developed in this work, shown schematically in Figure 1.9, are also based on DBR gratings in InP waveguides. The principle of operation is very similar to that shown above. A narrowband DBR-based filter separates the on-resonance wavelength from the express channels. The DBR-filter is integrated with a directional coupler that takes care of the spatial separation of the drop channel and the express channels. It will be shown that with conventional uniform DBR gratings, it is exceedingly difficult to implement filters and ADMs with a bandwidth sufficiently narrow for dense WDM applications. Similar devices have been demonstrated both in a structure with the grating filter at the center of the directional folder [37, 38] and in a folded structure [24], with filter bandwidth of 7 nm and 0.8 nm, respectively. Same architecture has been implemented in SiO2 on Si [39], with a bandwidth of 1.5 nm.

In this work an approach using DBR filters with one or more $\lambda/4$-shifts is demonstrated. By including $\lambda/4$-shifts in the DBR gratings, notch filters with very narrow bandwidth can be realized with good tolerance to material and process parameters. The bandwidth of the filters is limited only by the waveguide propagation loss. Finally, it will be shown that by including multiple $\lambda/4$-shifts, specified filter shapes can be obtained. By integrating these filters with directional couplers, tunable, narrowband Add-Drop Multiplexers can be implemented. With the potential for integration with other photonic devices, and their short

reconfiguration time, they are prime candidates for cheap, compact and versatile elements with applications in packet-switched optical WDM-networks.

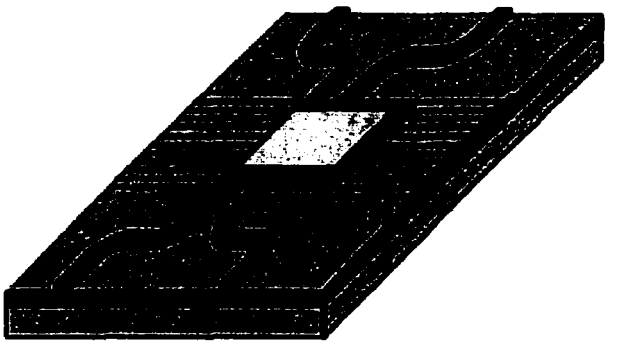

***Figure 1.9** Schematic representation of InP add-drop multiplexer implemented by integration of a narrow band DBR filter with a directional coupler.*

1.4 Organization of dissertation

The following chapter covers the filter design for the ADMs, that is, synthesis of the filter function and ADM parameters from the design requirements. The fundamental theory is covered, followed by a review of the analytical and numerical methods used for design and simulation. Based on the models, the filter parameters are calculated, and the expected device performance is described.

In Chapter 3 the abstract design from the previous chapter is translated into relevant, physical device parameters. The chapter covers epi-, waveguide- and directional coupler design, and sensitivity to material and processing parameter

variations. It also describes in some detail the fabrication procedures, with specific focus on the critical and non-trivial steps.

Chapter 4 contains the measured performance of the fabricated devices. The measurement set-up and procedure are described, followed by the experimental data. The experimental results are compared to the expected, calculated device characteristics.

The final chapter discusses suggestions for future work, both in terms of ideas to solve the problems with the current structure, along with suggestions for more complex devices with higher functionality. Finally, the chapter and dissertation are concluded with a summary and discussion.

References

[1] K. Okamoto, K. Takiguchi, and Y. Ohmori, "16-channel optical add/drop multiplexer using silica-based arrayed-waveguide gratings," *Electronics Letters*, vol. 31, pp. 723-4, 1995.

[2] K. Okamoto, M. Okuno, A. Himeno, and Y. Ohmori, "16-channel optical add/drop multiplexer consisting of arrayed-waveguide gratings and double-gate switches," *Electronics Letters*, vol. 32, pp. 1471-2, 1996.

[3] K. Okamoto, K. Syuto, H. Takahashi, and Y. Ohmori, "Fabrication of 128-channel arrayed-waveguide grating multiplexer with 25 GHz channel spacing," *Electronics Letters*, vol. 32, pp. 1474-6, 1996.

[4] T. Saida, A. Kaneko, T. Goh, M. Okuno, A. Himeno, K. Takiguchi, and K. Okamoto, "Athermal silica-based optical add/drop multiplexer consisting of arrayed waveguide gratings and double gate thermo-optical switches," *Electronics Letters*, vol. 36, pp. 528-9, 2000.

[5] K. Takada, H. Yamada, and K. Okamoto, "320-channel multiplexer consisting of 100 GHz-spaced parent AWG and 10 GHz-spaced subsidiary AWGs," *Electronics Letters*, vol. 35, pp. 824-6, 1999.

[6] H. Takahashi, K. Okamoto, and Y. Inoue, "Arrayed-waveguide grating wavelength multiplexers for WDM systems," *NTT Review*, vol. 10, pp. 37-44, 1998.

[7] M. Zirngibl, C. H. Joyner, and B. Glance, "Digitally tunable channel dropping filter/equalizer based on waveguide grating router and optical amplifier integration," *IEEE Photonics Technology Letters*, vol. 6, pp. 513-15, 1994.

[8] T. Takada, M. Abe, M. Shibata, M. Ishii, and K. Okamoto, "Low-Crosstalk 10-GHz-Spaced 512-Channel Arrayed Waveguide Grating Multi/Demultiplexer Fabricated on a 4-in Wafer," *IEEE Photonics Technology Letters*, vol. 13, pp. 1182-4, 2001.

[9] M. Kohtoku, S. Oku, Y. Kadota, Y. Shibata, and Y. Yoshikuni, "Polarisation-insensitive semiconductor arrayed waveguide grating integrated with spotsize converter," *Electronics Letters*, vol. 36, pp. 1055-6, 2000.

[10] H. H. Yaffe, C. H. Henry, M. R. Serbin, and L. G. Cohen, "Resonant couplers acting as add-drop filters made with silica-on-silicon waveguide technology," *Journal of Lightwave Technology*, vol. 12, pp. 1010-14, 1994.

[11] C. Kostrzewa and K. Petermann, "Bandwidth optimization of optical add/drop multiplexers using cascaded couplers and Mach-Zehnder sections," *IEEE Photonics Technology Letters*, vol. 7, pp. 902-4, 1995.

[12] B. J. Offrein, F. Horst, G. L. Bona, H. W. M. Salemink, R. Germann, and R. Beyeler, "Wavelength tunable 1-from-16 and flat passband 1-from-8

add-drop filters," *IEEE Photonics Technology Letters*, vol. 11, pp. 1440-2, 1999.

[13] H. Herrmann, A. Modlich, T. Muller, and W. Sohler, "Double-stage, integrated, acousto-optical add-drop multiplexers with improved crosstalk performance," 1997.

[14] H. Herrmann, A. Modlich, T. Muller, W. Sohler, and F. Wehrmann, "Advanced integrated, acousto-optical switches, add-drop multiplexers and WDM cross-connects in LiNbO/sub 3," 1997.

[15] R. Gaudino and D. J. Blumenthal, "A novel AOTF-based multichannel add-drop node and its cascadability in WDM ring networks," 1997.

[16] J. L. Jackel, M. S. Goodman, J. E. Baran, W. J. Tomlinson, G. K. Chang, M. Z. Iqbal, G. H. Song, K. Bala, C. A. Brackett, D. A. Smith, R. S. Chakravarthy, R. H. Hobbs, D. J. Fritz, R. W. Ade, and K. M. Kissa, "Acousto-optic tunable filters (AOTFs) for multiwavelength optical cross-connects: crosstalk considerations," *Journal of Lightwave Technology*, vol. 14, pp. 1056-66, 1996.

[17] D. A. Smith, R. S. Chakravarthy, Z. Bao, J. E. Baran, J. L. Jackel, A. d'Alesandro, D. J. Fritz, S. H. Huang, X. Y. Zou, S. M. Hwang, A. E. Willner, and K. D. Li, "Evolution of the acousto-optic wavelength routing switch," *Journal of Lightwave Technology*, vol. 14, pp. 1005-19, 1996.

[18] N. A. Riza and J. Chen, "Ultrahigh -47-dB optical drop rejection multiwavelength add-drop filter using spatial filtering and dual bulk acousto-optic tunable filters," *Optics Letters*, vol. 23, pp. 945-7, 1998.

[19] F. Wehrmann, C. Harizi, H. Herrmann, U. Rust, W. Sohler, S. Westenhofer, L. Shi, L. H. Spiekman, and X. J. M. Leijtens, "Fully packaged, integrated optical, acoustically tunable add-drop-multiplexers in LiNbO/sub 3," 1995.

[20] B. E. Little, S. T. Chu, H. A. Haus, J. Foresi, and J.-P. Laine, "Microring Resonator Channel Dropping FIlters," *IEEE Journal of Lightwave Technology*, vol. 15, pp. 998-1005, 1997.

[21] J. V. Hryniewicz, P. P. Absil, B. E. Little, R. A. Wilson, L. G. Joneckis, and P.-T. Ho, "Microring resonator notch filters," presented at Conference on Lasers and Electro-Optics, San Francisco, CA, USA, 2000.

[22] S. T. Chu, B. E. Little, P. Wugen, T. Kaneko, and Y. Kokubun, "Cascaded microring resonators for crosstalk reduction and spectrum cleanup in add-drop filters," *IEEE Photonics Technology Letters*, vol. 11, pp. 1423-5, 1999.

[23] S. T. Chu, B. E. Little, W. Pan, T. Kaneko, S. Sato, and Y. Kokubun, "An eight-channel add-drop filter using vertically coupled microring resonators over a cross grid," *IEEE Photonics Technology Letters*, vol. 11, pp. 691-3, 1999.

[24] R. C. Alferness, L. L. Buhl, M. J. R. Martyak, M. D. Divino, C. H. Joyner, and A. G. Dentai, "Narrowband GaInAsP/InP waveguide grating-folded

directional coupler multiplexer/demultiplexer," *Electronics Letters*, vol. 24, pp. 150-1, 1988.

[25] S. Fischer, M. Dulk, E. Gamper, W. Vogt, W. Hunziker, E. Gini, H. Melchior, A. Buxens, H. N. Poulsen, and A. T. Clausen, "All-optical regenerative OTDM add-drop multiplexing at 40 Gb/s using monolithic InP Mach-Zehnder interferometer," *IEEE Photonics Technology Letters*, vol. 12, pp. 335-7, 2000.

[26] F. Heismann, L. L. Buhl, B. I. Miller, M. Newkirk, U. Koren, M. G. Young, and R. C. Alferness, "Polarization-independent wavelength filter using a grating-assisted vertical directional coupler in InP," 1993.

[27] M. Horita, S. Tanaka, H. Furuya, and Y. Matsushima, "A tunable and narrow-band optical add and drop multiplexer utilizing coupled semiconductor waveguides and a striped thin-film heater," 1997.

[28] M. Horita, Y. Matsushima, T. Miyakawa, H. Taga, S. Akiba, H. Tanaka, K. Goto, M. Kuwazuru, and K. Tatekura, "Highly reliable optical add and drop multiplexer using a fiber grating and optical circulators," 1997.

[29] M. Horita, S. Tanaka, and Y. Matsushima, "Wavelength tunable optical add and drop multiplexer utilising coupled semiconductor waveguides and a striped thin-film heater," *Electronics Letters*, vol. 34, pp. 2240-1, 1998.

[30] M. Horita, S. Tanaka, and Y. Matsushima, "Sidemode suppression of optical add-and-drop multiplexer utilizing vertically coupled InGaAsP waveguides," 1999.

[31] Y. Shibata, S. Oku, Y. Kondo, T. Tamamura, and M. Naganuma, "Semiconductor monolithic add-drop multiplexer using a grating switch integrated with coupler structure," *Electronics Letters*, vol. 35, pp. 489-91, 1999.

[32] S. Tanaka, K. Utaka, T. Yamamoto, M. Horita, and Y. Matsusbima, "Proposal of new narrow-band wavelength filter using grating-assisted vertical contra-directional coupler," 1996.

[33] C. G. M. Vreeburg, T. Uitterdijk, Y. S. Oei, M. K. Smit, F. H. Groen, J. J. G. Van Der Tol, P. Domeester, and H. J. Frankena, "Compact integrated InP-based add-drop multiplexer," 1996.

[34] C. G. M. Vreeburg, T. Uitterdijk, Y. S. Oei, M. K. Smit, F. H. Groen, E. G. Metaal, P. Demeester, and H. J. Frankena, "First InP-based reconfigurable integrated add-drop multiplexer," *IEEE Photonics Technology Letters*, vol. 9, pp. 188-90, 1997.

[35] J. P. Weber, B. Stoltz, M. Dasler, and B. Koek, "Four-channel tunable optical notch filter using InGaAsP/InP reflection gratings," *IEEE Photonics Technology Letters*, vol. 6, pp. 77-9, 1994.

[36] J. P. Weber, B. Stoltz, and O. Oberg, "Integrated tunable polarization-independent channel dropping filter on InP for WDM systems," 1996.

[37] Y. Shibata, S. Oku, Y. Kondo, T. Tamamura, and M. Naganuma, "Semiconductor Monolithic Wavelength Selective Router using a Grating

Switch Integrated with a Directional Coupler," *IEEE Journal of Lightwave Technology*, vol. 14, pp. 1027-32, 1996.

[38] Y. Shibata, S. Oku, Y. Kondo, and T. Tamamura, "Semiconductor monolithic wavelength selective router using grating switch integrated with directional coupler," *Electronics Letters*, vol. 31, pp. 966-7, 1995.

[39] D. Mechin, P. Grosso, and D. Bose, "Add-Drop Multiplexer with UV-Written Bragg Gratings and Directional Coupler in SiO2-Si Integrated Waveguides," *IEEE Journal of Lightwave Technology*, vol. 19, pp. 1282-6, 2001.

Chapter 2 Design and modeling of DBR filters and integrated filter/directional coupler Add/Drop Multiplexers

2.1 Introduction

This chapter deals with the design of filters and Add-Drop Multiplexers and the numerical model used for design. The section following this introduction reviews the performance parameters for communications applications, and how these translate into requirements to device parameters. The following section outlines the problem and discusses the fundamental theory for DBR filters and directional couplers as applied to this work.

The main section of this chapter contains the results of the calculations, i.e. the design curves and the predicted performance of the device. Design trade-offs are discussed and sensitivity to device parameters is investigated. It is shown that the basic first-order filters are insufficient to achieve the required performance in the presence of waveguide loss, and an alternative method based on higher order filters is demonstrated.

The chapter is concluded with a review of the final design and the expected performance, followed by a brief summary of the entire chapter.

2.2 System requirements and design goals

Before discussing the basic design process and requirements to the device performance, a review of the basic principle of operation of the ADM is useful. For convenience, the schematic of the proposed device is shown in Figure 2.1. The device consists of two main functions: A narrowband DBR filter to select one channel, and a directional coupler to separate the selected channel from the multi-channel input. Without the directional coupler, the reflected channel (the drop channel) would appear on the input port, making expensive external optical circulators necessary. The specifics of the two device functions and issues relating to the integration of the two will be covered in more detail in a later section of this chapter.

In order to determine the requirements for device performance, it is necessary to consider the network application, and how the network requirements translate into device design goals.

The first issue is network channel spacing. Currently WDM systems with 50 GHz channel spacing are commercially available and are being widely deployed. For a reconfigurable (tunable) ADM device, this means that the optical filter bandwidth must be less than 50 GHz, as illustrated in Figure 2.1. Exactly how much less is determined by the actual filter shape and the cross-talk requirements, discussed below. For systems with even smaller channel spacing, the filter requirements are modified accordingly. In this demonstration of concept, the goal is a filter performance compatible with 100 GHz channel spacing.

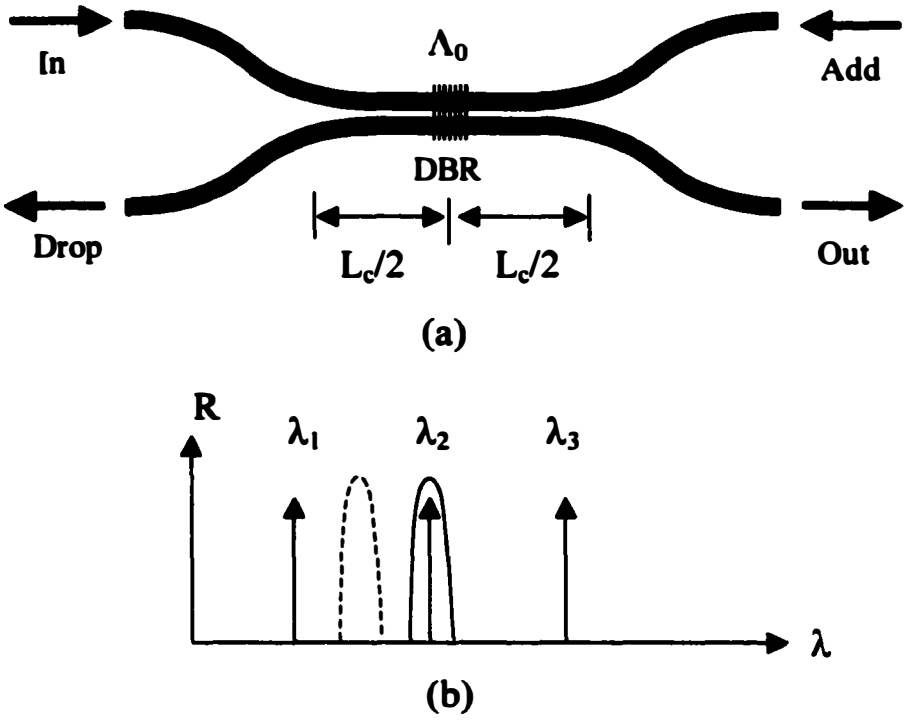

Figure 2.1. *(a) shows a device schematic. (b) illustrates the function of the filter, and the requirements to filter bandwidth in a tunable device. To fit the filter reflection band between two channels (dashed) the filter bandwidth must be substantially less than the channel spacing.*

For most applications, the device performance must be compatible with cascading a number of ADMs. Obviously, one important issue for cascadeability is fiber-to-fiber loss. Excessive device loss will limit the number of devices that can be cascaded without amplification. Fiber-to-fiber loss consists of several components: fiber-to-waveguide coupling loss, waveguide propagation loss, and finally, loss due to non-ideal filter and coupler characteristics. The first of these

components depends on the waveguide design, and can be minimized by depositing anti-reflection coatings on the device facets and by incorporating tapered mode converters to improve the matching between the waveguide mode and the fiber mode.

As discussed later in the section on filter design, waveguide propagation loss in the filter part of the device is a key parameter limiting the performance of the device in terms of filter bandwidth and cross-talk. This means that the maximum acceptable propagation loss is determined by filter design considerations, rather than the goal of minimizing fiber-to-fiber loss. For the S-bends, the design becomes a trade-off between acceptable wafer area, radiation loss and linear propagation loss/absorption. The losses in the S-bends consist of two components: Waveguide propagation loss, which is proportional to the waveguide length, and the radiation loss, increasing with decreasing radius of curvature.

The final loss component is non-ideal filter and coupler performance. The former causes not only excess device loss but is also an important factor determining the channel cross-talk. In contrast, assuming back reflections to the input ports are acceptable (either because an isolator is present, or because the system is tolerant to these reflections), the deviations from perfect 100% coupling in the directional couplers will merely increase the total device loss, but not cause cross-talk.

While loss is certainly an important consideration for scalability and cascadeability, it is a limit that can be overcome by amplification. In reality, channel cross-talk is more likely to be the limiting factor to device performance and cascadeability. It is

difficult to set a general number for maximum acceptable cross-talk, as it will depend on system design and parameters. At least –20 dB isolation is necessary for a single device, and probably –30 dB is required for a device in a system with cascaded Add-Drop nodes. For this work –20dB will be used as a design goal for maximum acceptable cross-talk.

The shape of the filter transfer function, including the phase characteristics, has not been discussed so far. It is harder to quantify these issues, and they will be addressed in a later section when the modeling results are presented and discussed.

In summary, while the actual requirements depend on system design and application, for the purpose of the design phase of this project, the following design goals were used: For loss, the acceptable waveguide loss is determined by the requirements to filter performance. From the calculations below, it will be clear that the total fiber-to-fiber losses will be dominated by coupling losses, which are outside the scope of this work. For cross-talk, we require an isolation better than –20 dB for a 100 GHz channel spacing, that is, the isolation must be better than –20dB at 50 GHz offset from resonance. When design trade-offs are necessary, priority is given to minimizing cross-talk.

In the simplest versions of the device, the performance can be modeled using either coupled-mode equations or the transfer-matrix method. While the coupled-mode equation method is relatively easy to implement and efficient for simple

structures, the computational load increases very fast with increasing complexity of the modeled structure. Each transition between filter sections or between coupler and filter requires another set of boundary conditions. Instead the transfer-matrix method was used; for a simple structure the coupled-mode equations were integrated to verify the results of the transfer-matrix calculations.

The necessary building blocks for a transmission matrix model of the ADM are given in literature [1], and will not be covered in any detail here. The required elements are the transmission matrices for a homogeneous waveguide (phase + loss), an interface between to propagation constants (reflection/transmission) and two coupled waveguides, characterized by the coupling coefficient. The model was implemented using Mathematica and Matlab software.

2.3 Modeling results

As explained in the introduction part of this chapter, the first step in the design is to develop and design an abstract design, i.e. from the device requirements calculate the filter and coupler parameters. In next chapter, these parameters are translated into actual physical device parameters.

The starting point for the design is the simple structure shown in Figure 2.1.a, consisting of two coupler arms with a DBR grating in the center of each arm. To minimize the computational effort and simplify the design process, it is desirable to separate the filter design and the coupler design. Conceptually the coupler design is relatively simple; we defer this for a later section. Therefore, we first

consider a simple model of a single waveguide with a DBR grating. The initial device design is based on a uniform grating, with the response approximately given by the analytical expressions:

$$\Delta f_s \approx \frac{\kappa v_g}{\pi}$$
$$r \approx \tanh(\kappa L)$$

Where Δf_s is the stopband bandwidth, r is the filter peak reflectivity, κ is the grating coupling factor, and v_g is optical propagation velocity.

To pick out a single channel in a dense-WDM system, the filter bandwidth is required to be less than ~50 GHz. The reflectivity should be greater than 99% to maintain good (better than –20dB) cross-talk isolation. From these requirements, we get a grating coupling factor of $<16cm^{-1}$, and a length of at least 1.6mm. The response of a filter with these parameters is shown in Figure 2.2. While this filter satisfies the initial requirements, the very low coupling factor is prohibitively difficult to fabricate in a reproducible and controlled way. Furthermore, two other problems exist; first, the high sidelobes will cause channel cross-talk from the through channels to the drop channel [2]. To avoid this cross-talk, the side-lobes must be suppressed, e.g. by using an apodized grating, which in turn requires the total grating length to be increased to maintain an acceptable peak reflectivity.

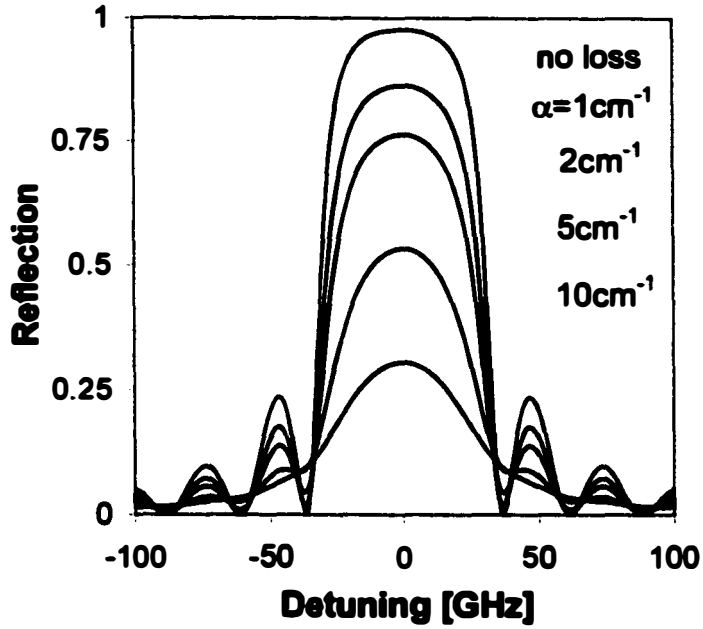

Figure 2.2 *Reflection characteristics for uniform DBR filter with $\kappa=16cm^{-1}$ and $L=1.6mm$. Also shown are the characteristics in presence of waveguide loss.*

Another problem is also illustrated in Figure 2.2, which includes the filter response in the presence of waveguide propagation loss. Because of the length of the grating, the response is highly sensitive to waveguide loss, and a rapid deterioration of the filter performance with increased loss parameter is observed.

Based on the preceding design example, it can be concluded that the simple uniform DBR grating filter is not a plausible structure for the OADM. Instead, a modified approach is proposed, based on λ/4-shifted DBR filters.

Narrow band filters and optical add-drop multiplexers based on λ/4 shifted DBR gratings.

As it was shown above, the simple uniform DBR filter is unsuitable for implementation of filters and ADMs with the required bandwidth. Instead an approach based on λ/4-shifted resonators is used. Figure 2.3 shows the calculated response of a uniform DBR grating and that of a λ/4-shifted DBR, with the same coupling coefficient κ (150 cm^{-1}) and total length L (300μm). The main difference is a very narrow notch at the DBR resonance frequency. This notch can be used to select a single channel to drop, while the express channels are reflected in the stopband. With this approach the problem of filter side-lobes is avoided, since only the part of the spectrum within the stopband is utilized. This is also the main limitation of this structure: The total channel count available in the system is now limited by the total width of the stopband. Methods to overcome this limitation are discussed in Chapter 5.

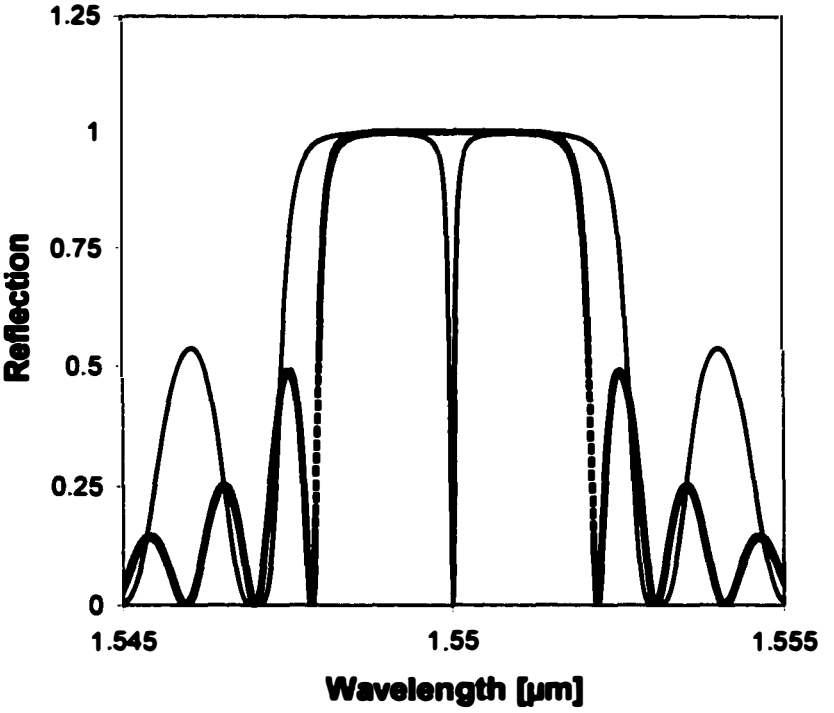

Figure 2.3 *Reflection characteristics for uniform (dashed) and λ/4-shifted DBR (fine line) filter.*

As with the simple DBR filter, approximate analytical expressions for the response can be derived [3, 4]:

$$\Delta f_s \approx \frac{\kappa v_g}{\pi}$$

$$\Delta f_t \approx \frac{2 v_g \kappa}{\pi} \exp(-2\kappa L)$$

$$r \approx \tanh(\kappa L)$$

where Δf_s is the stopband bandwidth, κ is the grating coupling factor, v_g is the optical velocity, Δf_t is the notch bandwidth, and r is the reflection coefficient.

The exponential dependency of κL on notch bandwidth shows the potential for very narrow filters. The goal is to maximize the peak reflectivity and the stopband bandwidth, while achieving the correct bandwidth of the center notch. The analytical equations form the initial starting point for the design; using the design goals of a stopband bandwidth of 800 GHz and a notch bandwidth of 25 GHz, the parameters are grating coupling coefficient κ=275 cm^{-1}, and total grating length L=300μm. Analysis using the transfer matrix method reveals that not only is the bandwidth of this design substantially smaller than 25 GHz, it is also very sensitive to even small values of waveguide loss. Based on a numerical investigation of the parameter space, Figure 2.4 and Figure 2.5, the optimum compromise between stopband bandwidth, notch bandwidth and sensitivity to waveguide loss was determined to be κ=150 cm^{-1} and L=300μm. The filter parameters for this design are a stopband bandwidth of 650 GHz, and a notch bandwidth of 15 GHz. The response is shown in Figure 2.6, also showing the response when propagation loss is included. As expected for a high-Q filter, the response deteriorates rapidly with increasing loss, again underscoring the need for very low loss waveguides.

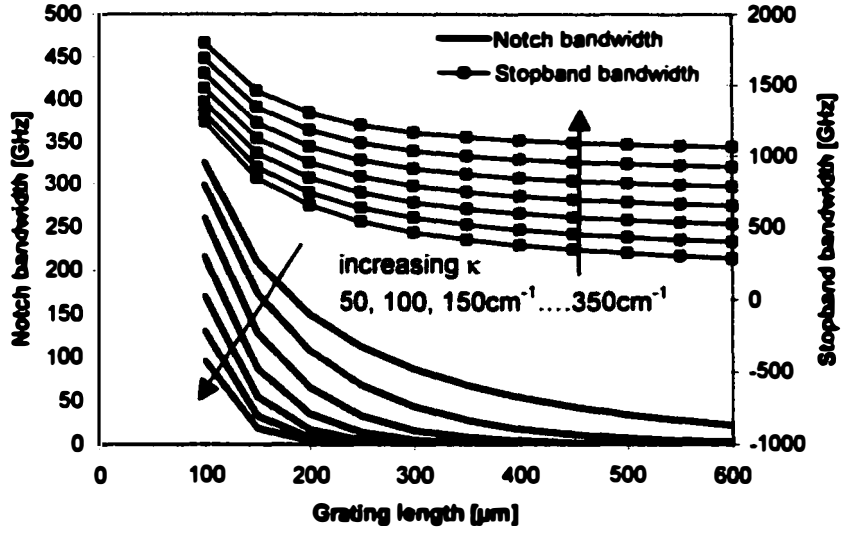

Figure 2.4 *Stopband and notch filter bandwidth for quarterwave-shifted DBR filter.*

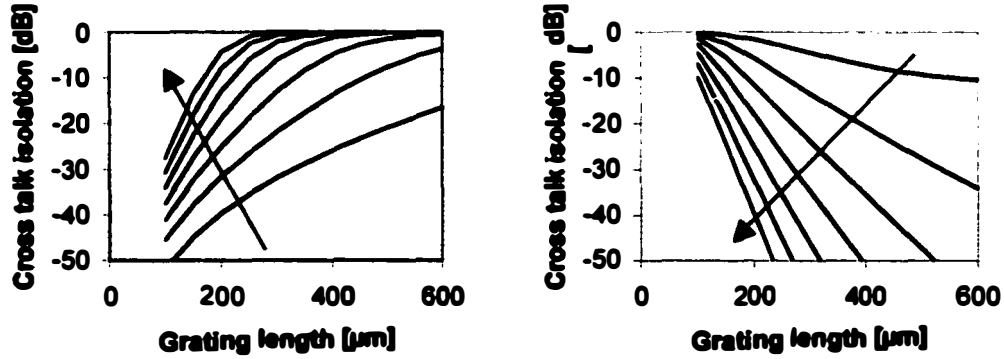

Figure 2.5 *Filter cross-talk isolation with moderate ($2cm^{-1}$) waveguide propagation loss. Both buss-to-drop (left) and drop-to-bus cross-talk are shown. The arrows indicate the direction of increasing grating coupling coefficient κ, in steps of $50cm^{-1}$ starting at $50cm^{-1}$.*

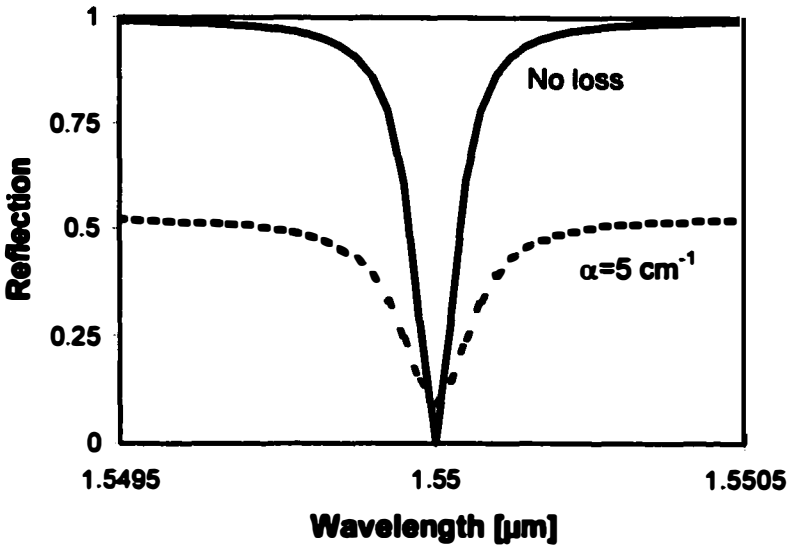

Figure 2.6 *Notch filter characteristics in ideal, loss-less filter and in filter with 5 cm^{-1} loss coefficient*

As the figure clearly shows, the decrease in filter-Q increases the notch bandwidth, and – more important – it causes increasing channel cross-talk. This is summarized in Figure 2.7, for the design shown in Figure 2.6. To maintain better than 20 dB isolation, the waveguide propagation loss must be kept below 1.5 cm^{-1} (6.5 dB/cm). The low-loss requirement puts high demands on both design and fabrication. This will be discussed in the following chapter.

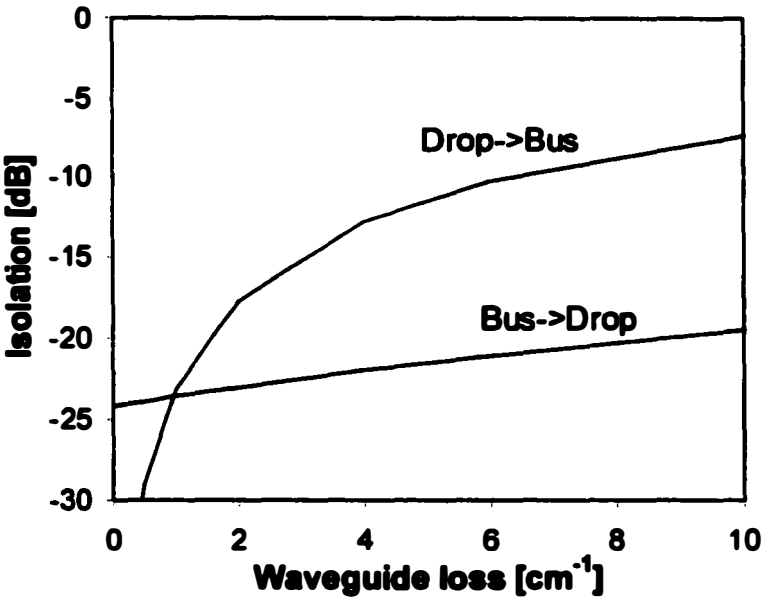

Figure 2.7 *Filter isolation as function of waveguide propagation losses*

The previous design example was calculated in the simplest configuration: a simple filter in a waveguide, that is, completely neglecting the directional coupler in which the filter is embedded in the case of the ADM. In the ADM structure, two λ/4-shifted DBR resonators are placed in a pair of coupled waveguides, see Figure 2.1, causing coupling between the two resonators. This coupling causes a splitting of the eigen-states of the resonators, a phenomenon known from all types of degenerate, coupled resonators. Figure 2.8 shows an example of this, as calculated with the transfer-matrix method.

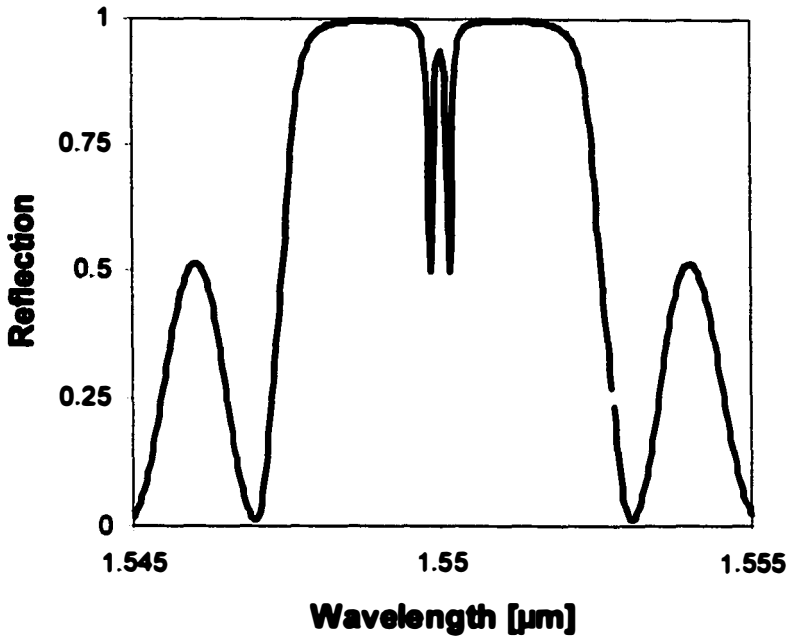

Figure 2.8 *Splitting of eigen-modes when the two waveguide DBR filters are coupled.*

The obvious way to avoid this effect is to de-couple the two resonators, most easily achieved by separating the waveguides in the filter region, illustrated in Figure 2.9. With this approach, not only is the coupling effect avoided, also one of the design constraints is removed, giving more freedom in the design. With the waveguides separated in the DBR section of the device, the design of the filter and directional coupler sections become completely decoupled, and can be solved as two separate problems. Consequently, the remainder of this chapter will focus on the filter design.

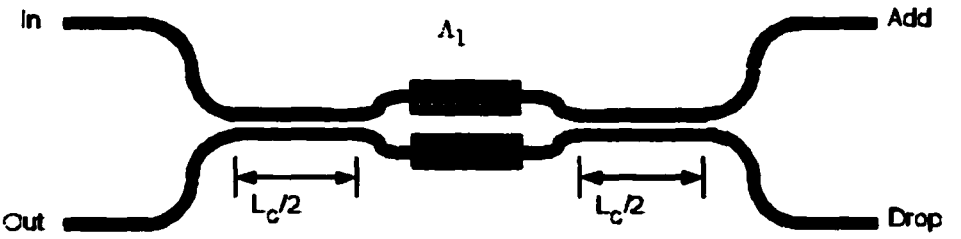

Figure 2.9 *Schematic of integrated ADM, with decoupled waveguides in the filter section.*

2.4 Higher-order filters

Even in the most robust design, the λ/4-shifted filters shown above are relatively sensitive to loss, making implementation difficult. Also the sharpness of the notch limits the information bandwidth of the channels and makes the filter performance highly sensitive to even minor deviations in signal wavelength or changes to device characteristics caused by environmental parameters. Another issue is the phase characteristics of the filter, shown in Figure 2.10. Around the resonance wavelength, the phase characteristics is highly non-linear, causing high, non-linear dispersion. This can cause distortion, which limits the number of devices that can be cascaded in a system.

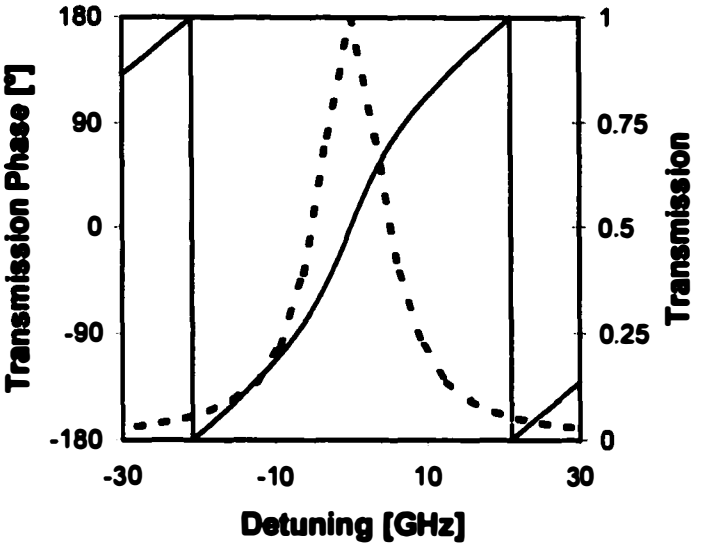

Figure 2.10 *Transmission phase (line) and amplitude (dashed) of λ/4 filter*

To avoid the dispersion, and to make the device more robust, it is desirable to have a wider, "flat" filter response at the bottom of the notch, while maintaining the steep slope. This can be achieved with higher-order filters, i.e. filters with several λ/4-shifts [4, 5]. This section deals with the design of higher-order filters.

Higher-order filters are well known from basic electronics LC and microwave filter theory, typically based on maximum-flat (Butterworth) or Chebyshev designs. By establishing the transformation from the λ/4-shifted DBR filter cascade, to LC-filters, the well-known design methods from electronic filters can be applied.

The design of the LC passband filters follow [6-8], and is based on transformation of prototype low-pass filters to passband filters with specified center and cut-off

frequencies. The resulting filter is a cascade of shunt resonators and series resonators.

The translation of the LC pass-band filter design to a multi-section λ/4-shifted DBR filter is described in the following [4, 8]. The starting point is the following equivalent circuit for a single-section DBR filter:

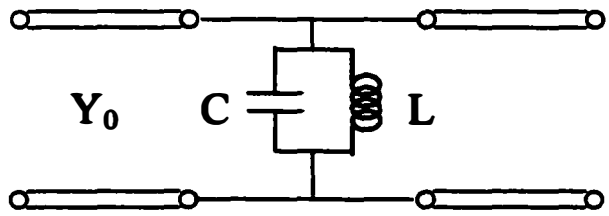

Figure 2.13. *Equivalent circuit for single-section λ/4-shifted DBR filter*

The one-sided external $Q_{E,1}$ of this LC resonator is given by

$$Q_{E,1} = \frac{\omega_0 C}{Y_0} \quad \Leftrightarrow \quad \frac{\omega_0}{Q_{E,1}} = \frac{Y_0}{C}$$

where ω_0 is the resonance frequency. The external Q of the DBR filter is given by:

$$\frac{\omega_0}{Q_{E,1}} = 2\kappa v_g \exp(-2\kappa l)$$

where l is the half-length of the λ/4 DBR resonator and v_g is the group velocity. Combining the two equations and generalizing to multiple sections with element values C_j and L_j derived from the LC-filter design the length of each of the DBR-filters can be calculated:

$$l_j = \frac{\ln(2\kappa v_g C_j)}{2\kappa}$$

The remaining step in the transformation from a LC pass-band filter to a filter based on cascaded DBR-resonators is illustrated in Figure 2.12. The λ/4-shifts between the cascaded resonators serve as impedance inverters, transforming LC shunt resonators to the series resonators required for the LC filter.

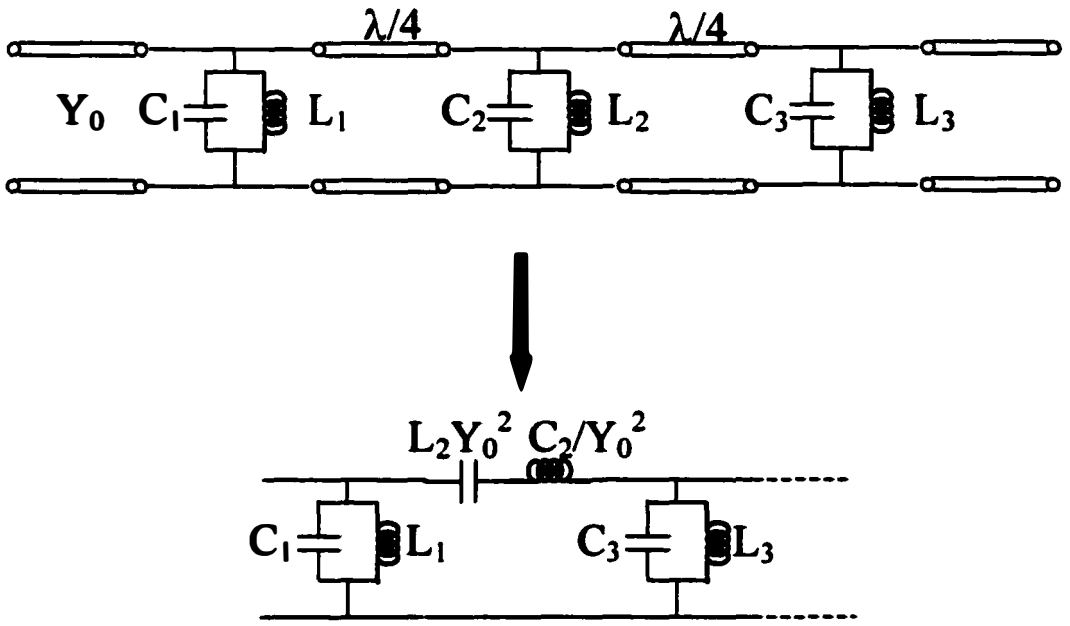

Figure 2.12. *Transformation of cascaded DBR-filters to prototype LC-filter through the use of quarterwave impedance inverters.*

The filter design procedure thus becomes:

1) Determine the number of sections required to achieve specified parameters for maximum pass-band reflection and maximum transmission outside the pass-band (filter skirt steepness) [6].
2) Design prototype low-pass filter with correct number of sections, using tables or analytical expressions.
3) Transform low-pass filter design to band-pass filter, using standard transformations[6].
4) Translate the LC band-pass filter design to DBR-section lengths using the equations given above.

In this remaining part of this section, the focus is on the DBR filter designs and design trade-offs, in relation to the DBR filter and ADM response.

In the general case, it is possible to design filters with different value of κ for the different stages, but for fabrication reasons this approach is not advantageous. Instead all stages have the same κ, but different lengths, l_j. A generalized filter is shown in Figure 2.13. The device specifications are notch bandwidth, stopband bandwidth, and filter shape and requirements (isolation at filter edge for Butterworth, ripple depth for Chebyshev filters).

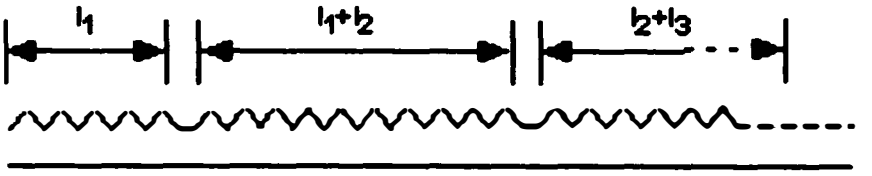

Figure 2.13 *Higher-order DBR filter*

The device parameters are the grating coupling factor, κ; and the length of the individual sections, l_i. As it was the case for the uniform DBR filter and the first order filters, the coupling coefficient determines the stopband bandwidth. The resonator lengths control the notch filter shape and bandwidth. The stopband reflection is determined by the κl product; for the third and fifth order filters here, the parameter values obtained from the previous mentioned design goals give better than 99% reflection (<-20dB transmission) in all cases, and it is not necessary to specifically consider this requirement.

Figure 2.14 shows designs of a fifth order Chebyshev filter with 0.1dB ripples, and a fifth order Butterworth filter, both designed for a 3dB bandwidth of 25 GHz and at least 20 dB isolation at 40 GHz offset. The total length of Chebyshev filter is 705μm, and the Butterworth filter is 690μm. This is compared to the length of the first-order filter of 300 μm.

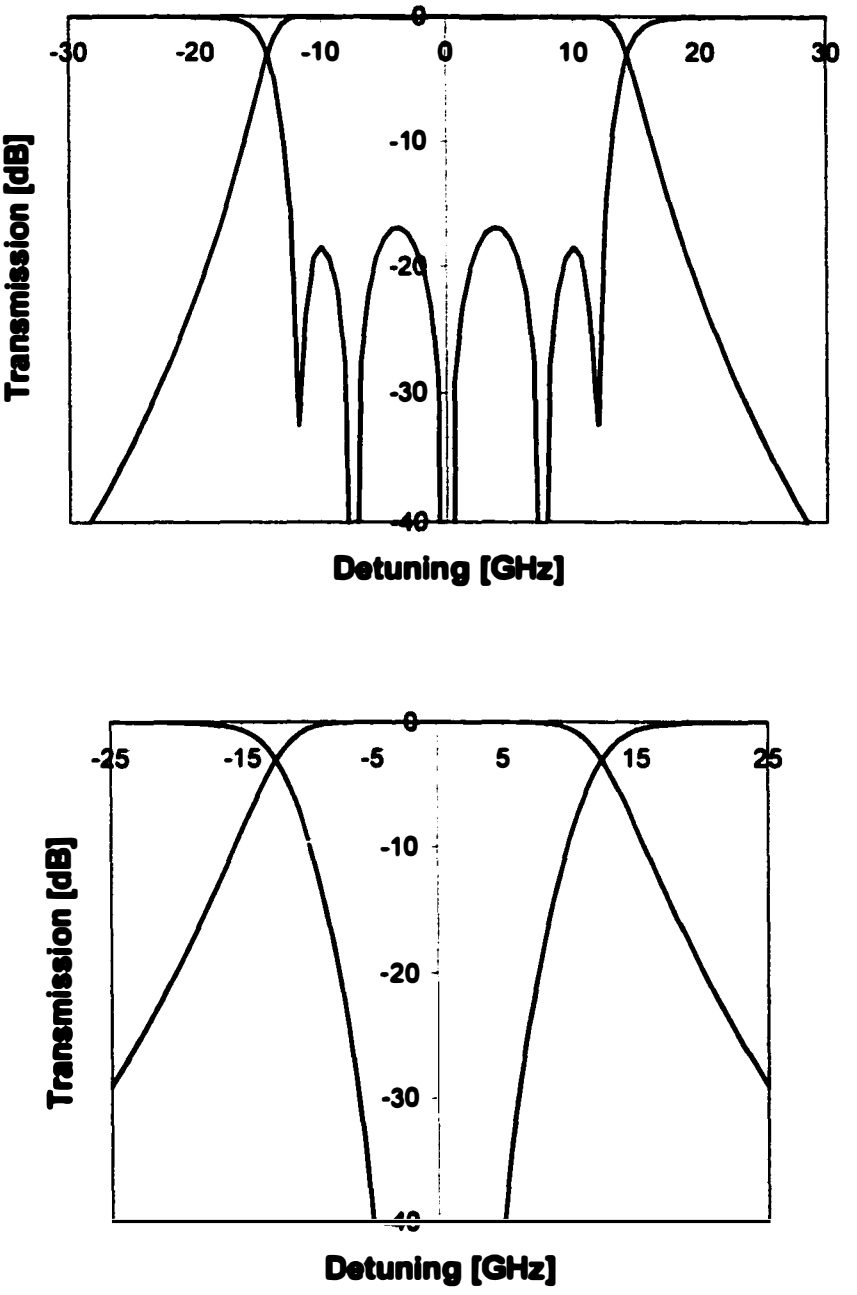

Figure 2.14 *Filter characteristics of fifth-order Chebyshev and Butterworth filters. Transmission and reflection are shown in both cases.*

As mentioned, the higher-order filters are much less sensitive to internal waveguide losses in the resonators, compared to the single λ/4-shifted filters in the previous section. This is illustrated in Figure 2.15, in comparison with Figure 2.6. Where the λ/4-filter required a loss coefficient below 1.5 cm^{-1} to maintain 20 dB cross-talk isolation, a fifth-order maximum-flat filter will meet that requirement up to loss coefficients of 15 cm^{-1}.

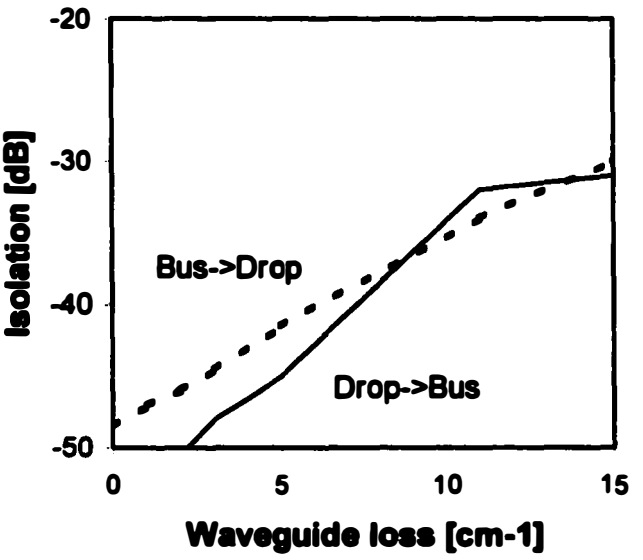

Figure 2.15 *Channel cross-talk of fifth-order maximum-flat filter.*

Another important aspect of the device performance and the impact of waveguide loss is the changes in filter shape, in particular the increase in pass-band bandwidth. In addition to the deviation from ideal caused by zero-bias propagation loss, loss is introduced when the filter is tuned by current injection. In other words, the filter

characteristics will change under operation. The simple first-order filter described in the previous section showed a high sensitivity to loss, a result that will be confirmed by experimental results in Chapter 4. We have already seen how the cross-talk performance of the fifth-order filters is far superior to that of the first-order $\lambda/4$-shifted filter. Figure 2.16 shows the characteristics of a fifth-order Butterworth filter for different values of waveguide loss. The calculation clearly proves that also the filter bandwidth sensitivity to loss is greatly reduced. However, the price of improvements in cross-talk and bandwidth sensitivity is a substantially higher insertion loss in the presence of waveguide loss. This is due to the length of the device – the fifth order filters being 2.5 times longer than the first-order version.

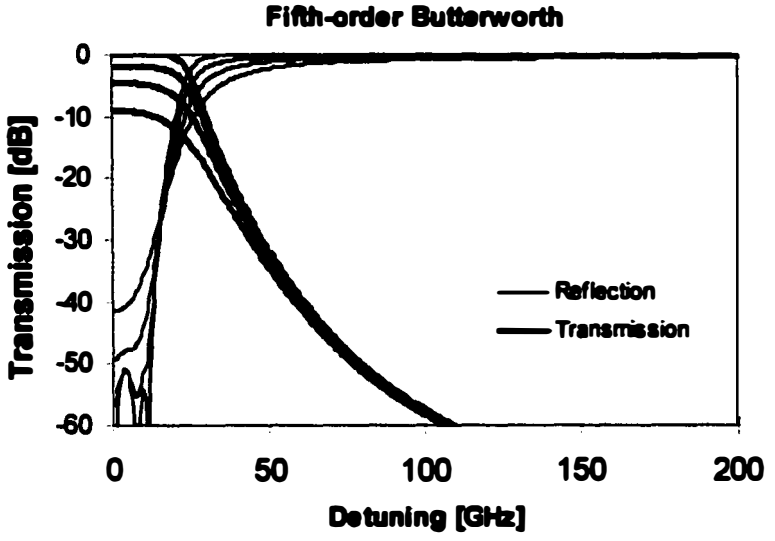

Figure 2.15 *Response of fifth-order Butterworth filter for waveguide loss of 0, 2, 5, and 10 cm^{-1}.*

From Figure 2.10 it can be seen that the Chebyshev filter does not meet the -20dB reflection in the pass-band. To meet that requirement, and at the same time have sufficient reflection at 50GHz and 100GHz detuning, a seven-section filter is required. For that reason, the Butterworth filters are better suited than the Chebyshev filters for application as a channel-separating filter. The seven-section design is more sensitive to waveguide losses, and has more non-linear phase characteristics, unsuitable for communications applications. Furthermore, the filter is substantially longer, which translates not only to increased complexity and device length, but also higher dispersion and higher insertion loss in the presence of propagation loss. Finally, the group delay dispersion, which is already worse for the Chebyshev filters than the Butterworth designs, increases with the number of filter stages [8]. This is particularly important in cases where the signal bandwidth is comparable to the filter bandwidth.

In contrast, the Butterworth filters are more robust against losses and other parameter variations, and particularly in the presence of loss, the phase characteristic is more suited for application as channel dropping filter, since it is closer to linear around the center wavelength, and therefore causes less signal distortion. This is illustrated in Figure 2.17, which shows the transmission phase characteristics of the fifth order Butterworth filter in the loss-less case.

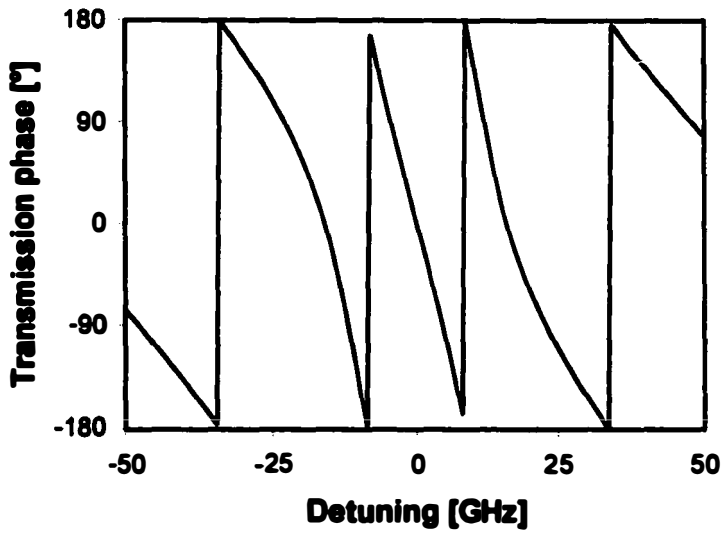

Figure 2.17 *Transmission phase of fifth-order 25 GHz bandwidth Butterworth filter.*

2.5 Summary

This chapter covered the design of narrow-band filters for channel dropping filters and integrated Add-Drop Multiplexers. It was shown that a simple DBR-filter based approach is practically impossible to implement, due to the stringent requirements to fabrication tolerances and waveguide propagation losses. An alternative approach, based on quarterwave-shifted DBR gratings was described. It was shown that this method is a plausible solution if the waveguide losses can be kept small. In the design derived in this chapter, it was found that the maximum acceptable loss is ~1.5 cm^{-1} to maintain cross-talk isolation better than 20 dB. The

filters have a design stopband bandwidth of 800 GHz and a notch passband bandwidth of ~15 GHz in the absence of loss.

Besides demonstrating the importance of maintaining low loss, the analysis also illustrated other problems with the simple first order version of the filters. First of all, the shape of the notch requires a very high degree of control of the signal wavelength and places strong requirements on the stability of the device to changes in environmental parameters. Any shift in device or signal center wavelength will cause a severe degradation in device performance. Furthermore, the sharpness of the notch limits the maximum optical bandwidth of the signal.

To overcome these problems, higher order filters were designed based on Chebyshev and Butterworth (maximally-flat) designs from the theory of LC- and microwave filters. With this approach it is possible to obtain high isolation and narrow bandwidth in a structure less sensitive to loss and parameter variations. A fifth-order maximum-flat filter with 25 GHz bandwidth and better than 20 dB isolation at 40 GHz offset was designed. With the steepness of the filter notch, the actual useful spectral width is higher than for a comparable first-order design, reducing the sensitivity to variations in signal wavelength and reducing the impact of small changes to device characteristics, e.g. due to environmental changes.

The following chapter takes these abstract designs and translates them to a physical device design. It also covers the integration with a directional coupler, to obtain a fully integrated ADM.

References

[1] L. A. Coldren and S. W. Corzine, *Diode Lasers and Photonic Integrated Circuits*. New York: John Wiley & Sons, Inc., 1995.

[2] Y. Shibata, S. Oku, Y. Kondo, and T. Tamamura, "Effect of Sidelobes on Demultiplexing of a Grating-Folded Directional Coupler Demultiplexer," *IEEE Photonics Technology Letters*, vol. 8, pp. 87-9, 1996.

[3] H. A. Haus, *Waves and fields in optoelectronics*. Englewood Cliffs, NJ 07632: Prentice-Hall, Inc., 1984.

[4] H. A. Haus and Y. Lai, "Theory of cascaded quarter wave shifted distributed feedback resonators," *IEEE Journal of Quantum Electronics*, vol. 28, pp. 205-13, 1992.

[5] H. A. Haus and Y. Lai, "Narrow-band distributed feedback reflector design," *Journal of Lightwave Technology*, vol. 9, pp. 754-60, 1991.

[6] G. L. Matthaei, *Microwave filters, impedance matching networks and coupling structures*. New York, NY: McGraw-Hill, Inc., 1964.

[7] P. A. Rizzi, *Microwave Engineering - Passive Circuits*. Englewood Cliffs, NJ 07632: Prentice-Hall, Inc., 1988.

[8] A. Melloni and M. Martinelli, "Synthesis of Direct-Coupled-Resonators Bandpass Filters for WDM systems," *IEEE Journal of Lightwave Technology*, vol. 20, pp. 296-303, 2002.

Chapter 3 – Device Design and Fabrication

3.1 Introduction

In the previous chapter, the design requirements and calculations for the filter were described, and device parameters, i.e. DBR filter lengths and grating coupling coefficients were determined. In this chapter, the focus is on the physical design and fabrication of the device – in other words, translating the abstract device design of the previous chapter into actual, physical device parameters.

First section deals with the design of the waveguide and the epi structure. In particular, the goal of minimizing the waveguide loss in the filter part of the device is emphasized. This section also covers the design of the coupler and grating.

Three sections deal with fabrication of the devices. Sections 3.3 and 3.4 describe the grating processing and preparation for regrowth, including the fabrication of a quarterwave-shifted grating; Section 3.5 covers the waveguide process and remaining device fabrication. The following section contains calculations on the tunability of the filters and ADMs, and discusses the limits and methods to improve tuning range. This is followed by a short summary of the chapter.

3.2 Epi and waveguide design.

This section covers the design process of the epitaxial structure and the waveguide design. Two slightly different basic structures are used, shown in Figure 3.1. In both cases an InGaAsP layer constitutes the waveguide through the entire device. The waveguide is kept undoped to minimize propagation loss. For the same reason, both designs include doping offset layers on both sides of the waveguide. The first and simplest design has the grating etched directly in the waveguide layer, maximizing the overlap between grating and optical mode, and optimizing the carrier injection efficiency for tuning. This was the first generation design fabricated. The problems with this design are control and reproducibility of the grating etch depth, and the quality of regrowth on the exposed InGaAsP waveguide surface. In contrast, the second design has a grating layer, separated from the main waveguide by a thin InP etch stop layer. Using a combination of dry etch and selective wet etch, much better control over the grating etch depth can be achieved. The advantages of this design are control of grating depth through epitaxy, and having regrowth on an InP surface, giving better material quality. The disadvantage of this structure is the InP stop etch layer's potential effect as an injection barrier to hole injection. These effects, and the advantages and disadvantages of the two structures will be covered in detail in the following.

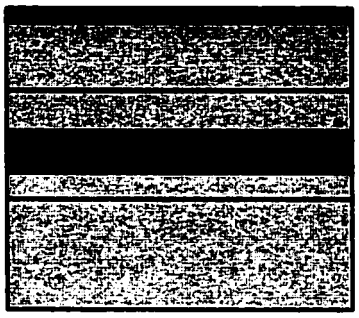

p+-InGaAs contact layer
p-InP (Zn:7e17)
uid InP doping set-back
uid 1.3Q InGaAsP waveguide
uid InP doping setback
n-InP substrate and buffer

Design 1

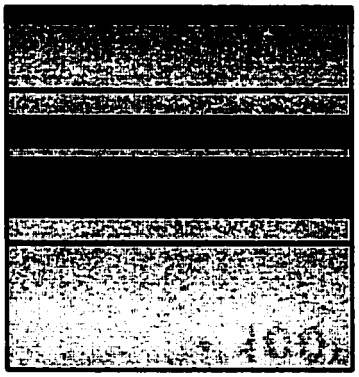

p+-InGaAs contact layer
p-InP (Zn:7e17)
uid InP doping setback
uid 1.3Q InGaAsP grating layer
uid InP stop-etch layer
uid 1.3Q InGaAsP waveguide
uid InP doping setback
n-InP substrate and buffer

Design 2

Figure 3.1. *Epitaxial waveguide structures for filters and ADMs*

An important result from the design calculations in the previous chapter is the significance of minimizing the propagation losses in the filter section of the Add-Drop Multiplexers. This will be an important priority through the entire design. Several effects contribute to the waveguide propagation loss: Free-carrier absorption in the doped layers, scattering from imperfect waveguides, scattering from the waveguide perturbations that form the DBR mirror, and inherent material

absorption. Radiation loss in the S-bends also contributes to the total chip loss, but not to the deterioration of the filter-Q.

The first design decision is on the waveguide material. Higher bandgap material gives less optical and carrier confinement and also reduces the tuning efficiency. In comparison the lower bandgap material yields higher index shift for the same injected carrier density, but also has higher optical loss. As demonstrated in the previous chapter, the propagation loss is the critical parameter in achieving the narrow filter bandwidth. Therefore, 1.3μm bandgap-wavelength material was chosen for waveguide and grating layers.

Here the design labeled as design 2 in Figure 3.1 is considered. Most of the discussion here applies equally to design 1. The thickness of the waveguide is determined by the following considerations: First, to avoid excessive absorption from free-carrier absorption in the doped cladding layers and to maximize tuning efficiency, the waveguide should be made thick enough to obtain good confinement, i.e. minimize the amount of optical field in the cladding layers. The losses from free carrier absorption can also be reduced by increasing the doping offset layer thickness, but this is done at the expense of increased resistance. Secondly, at the same time the design goal for the grating coupling factor κ should be met. Making the waveguide thicker increases the confinement, but reduces the overlap with the grating layer. This makes it necessary to increase the grating etch depth, which in turn increases scattering losses. Using one-dimensional slab

waveguide analysis, the waveguide confinement factor, effective index and grating confinement factor were calculated as function of waveguide thickness and grating etch depth. Using the following relationship [1], the grating coefficient can be calculated:

$$\kappa = \frac{4}{\pi}\frac{n_g}{\bar{n}}\frac{\pi}{\lambda}\Gamma_g \delta n_g$$

where n_g is average grating layer index, n- is the effective index, λ is the wavelength, Γ_g is the grating layer confinement and δn_g is the grating layer index perturbation.

The results are shown in Figure 3.2. Based on this a waveguide thickness of 3000 Å and a grating etch depth of 500 Å were used to achieve a grating coupling coefficient of 150 cm^{-1}.

Next the thicknesses of the doping offset layers are determined. With this basic structure as starting point, it is possible to calculate the propagation losses due to free-carrier absorption in the p- and n-cladding layers. Figure 3.3 shows the loss in the p-cladding and the resistance of the p-ridge vs. the doping offset thickness. The design trade-off here is the compromise between low loss and low forward series resistance in the device. Since the primary goal of this work is the development of very narrowband filters and ADMs, a relatively thick doping off-set layer was chosen, a value of 0.3μm was used, corresponding to a loss contribution of ~0.5cm^{-1}. Free-carrier absorption in the n-layers is significantly

smaller; on the n-side an offset thickness of 0.2 μm was used, corresponding to a loss-contribution of less than 0.1 cm^{-1}. Note that the calculated resistance is based on 7e17 p-doping in the doped part of the p-cladding. A different value or different doping profile will obviously yield another value of resistance for a given doping offset, but since the resistance in this calculation is dominated by the undoped layers, the results will not change substantially with a different p-doping level.

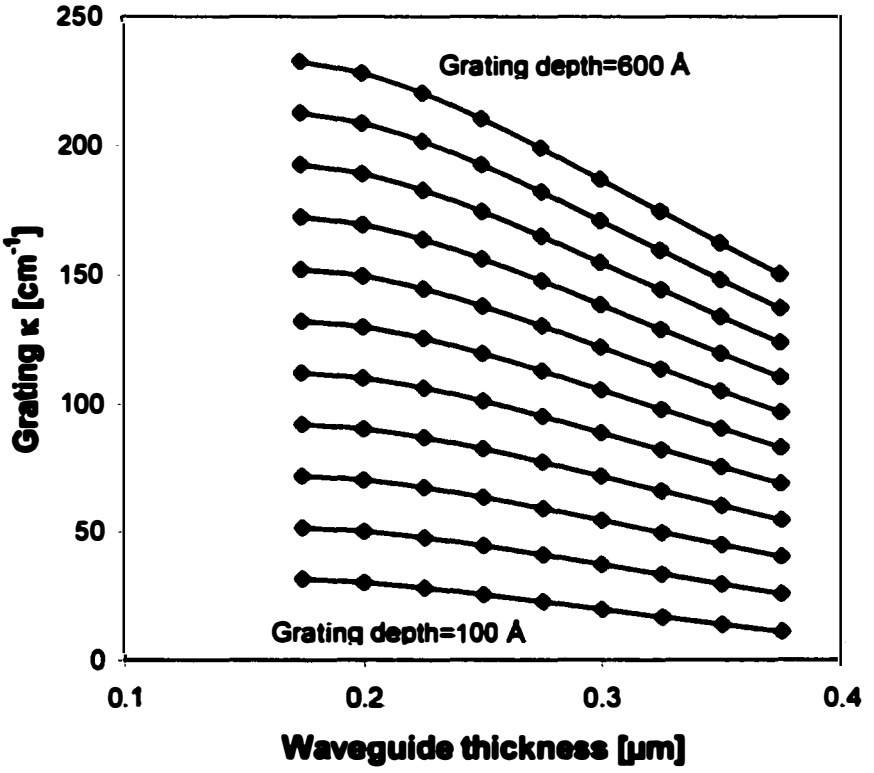

Figure 3.2 *Grating coupling coefficient as a function of waveguide thickness with grating depth as parameter. Grating depths from 100 Å to 600 Å are shown from bottom to top in steps of 50 Å.*

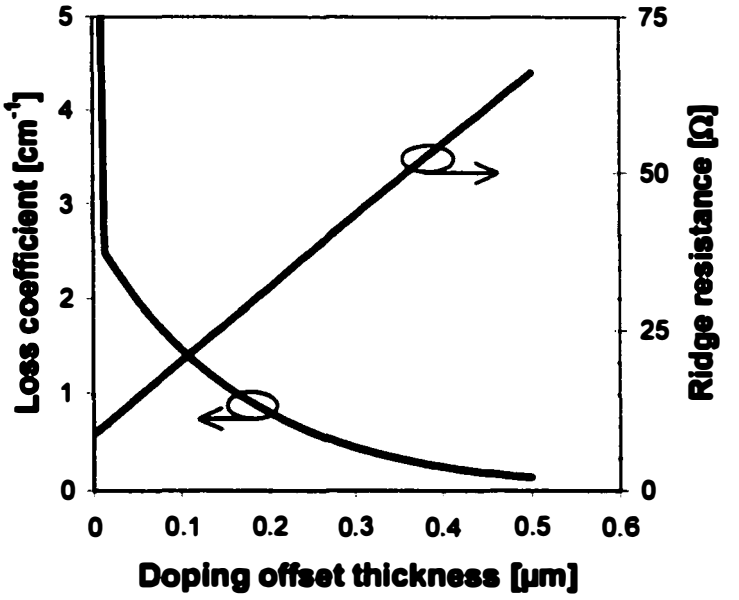

Figure 3.3 *Ridge resistance and loss contribution due to free-carrier absorption in p-cladding as functions of the p-doping offset layer thickness. The contact area is 150μm x 2.5 μm, and doping in the upper cladding is assumed 7e17 cm^{-3}.*

To finalize the waveguide design, the waveguide width is set to the maximum width where the waveguide remains single-mode. This width is ~2.5μm. Keeping the waveguide as wide as possible, maximizes the tuning range and minimized the effect of imperfect waveguide definition. The third concern when deciding the waveguide width is the coupler sensitivity to fabrication tolerances and variations. Using a commercial 3-D beam propagation software package (BeamPROP), the coupling length was calculated as function of waveguide width and spacing. With

a waveguide width of 2.5 μm and spacing of 1 μm, the coupling length is relatively insensitive to small variations in waveguide width, as long as the center-to-center distance is kept constant. At the same time, the total length is kept at a reasonable 1200 μm. The photolithographic definition of the waveguides and the waveguide etch may vary slightly from the photo mask design, due to under- or over-develop or variations in etch undercut, but in all cases the center-to-center spacing stays constant. Shorter coupling length requires smaller waveguide spacing, which is hard to process uniformly and reproducibly.

The calculations described above yield a coupling length of 1182 μm when the gradual coupling in the S-bends is neglected. In the final design, beam propagation calculations are used to adjust the coupler length to account for the S-bends.

To summarize the waveguide design, the final structure has a 3000 Å thick 1.3μm bandgap wavelength undoped InGaAsP waveguide, with a 500 Å thick grating layer of the same material. The doping offset is 0.3μm on the p-side and 0.2 μm on the n-side, giving an expected contribution to propagation loss from free-carrier absorption of 0.6 cm^{-1}. The waveguide width is set to 2.5 μm, with a waveguide spacing of 1μm in the coupler, to obtain a design that is robust against fabrication tolerances and variations.

With a waveguide spacing in the coupler section of 1 μm, the smallest practical spacing for fabrication, the coupling length becomes 1182 μm. S-bends with

lateral shift of 123.5 μm are used to separate the waveguides by 250 μm at the input and output.

Finally, in general the S-bend radius of curvature is determined by minimizing the sum of background propagation loss (increasing with radius) and radiation loss (decreasing with increasing radius). This procedure obviously requires a known value for the background propagation loss. Since a main objective in this work is minimizing the waveguide loss, a low value of 1.5 cm^{-1} for propagation loss was used to optimize the S-bends. BeamPROP was used to calculate the transmission through the S-bend versus the radius of curvature; this optimization yielded a design with 1700μm radius in the S-bends for a lateral displacement of 123.5 μm. In this initial design, a constant radius of curvature circle arc was used. Using a tapered, adiabatic design optimized with a measured value of propagation loss would be an improvement for future designs [2].

3.3 Grating fabrication

The DBR gratings in the filters and ADMs in this work are fabricated using a far-field holography process described below. Alternative methods include near-field holography using proximity exposure with a phase mask [3, 4], and direct write e-beam lithography. Compared to far-field holography, both of these methods are better suited for fabrication of λ/4-shifted gratings. Unfortunately, near-field

holography was not available or feasible at UCSB, and direct-write e-beam is time consuming, expensive and currently not a reliable option either. The problems using far-field holography will be described below, along with the solution.

The far-field holography process is illustrated in Figure 3.4. A thin layer of photo resist is spun uniformly over the entire sample. In this work diluted Shipley 1805 was used. Applied at 6000 rpm, this positive resist is ~600Å thick. Using the set-up in Figure 3.4 the resist is exposed with an interference pattern. The set-up consists of a HeCd laser with an emission wavelength of 325 nm, a beam expander and sample holder mounted on a rotation stage. The beam from the laser is expanded and collimated before hitting the mount, as shown. The mount is a 90° fixture with the sample holder on one side, and a UV mirror on the other. Part of the beam hits the sample directly, while another part of the collimated beam bounces of the mirror before hitting the sample. The two beams interfere on the sample surface and create a periodic pattern that exposes the resist. The period of the interference pattern is given by:

$$\Lambda = \frac{\lambda_{UV}}{2\sin(\alpha)}$$

where Λ is the period, λ_{uv} is the wavelength of the exposure laser, and α is the rotation angle of the sample mount, as defined in Figure 3.4.

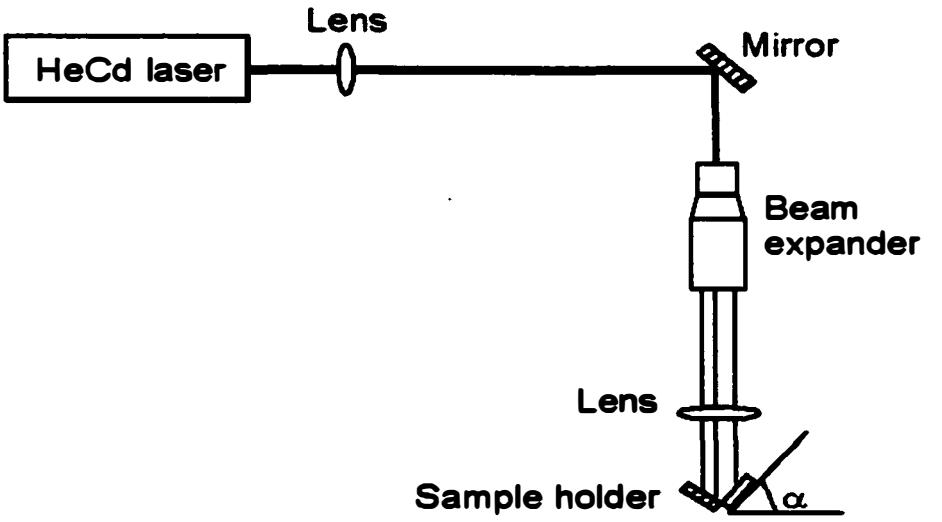

Figure 3.4 *Far-field holography exposure set-up for grating fabrication*

The grating pattern period can be verified by observing the diffraction angle of the first order diffraction from the surface after development. By using this method and running calibration runs before the actual sample, the desired grating pitch can be achieved with high accuracy. More detail on the far-field holography method of grating fabrication can be found in [5].

The periodic resist pattern formed in the manner described above can be transferred to the semiconductor by either wet or dry etch. For the first process run in this work, using the structure labeled "design 1" in Figure 3.1, the grating was wet etched, using a saturated bromine water (SBW) based etch. Using this approach, the etch was typically very non-uniform over the sample area. Also, the etch rate was not reproducible from one etch to another, making careful calibration

necessary before every etch. To avoid these problems, the gratings for "design 2" were etched using a combination of dry and wet etch.

For the dry etch process, a mask is required to protect areas without grating. For this mask, a thin layer of SiN is used. It is imperative to keep this layer as thin as possible, while still maintaining a sufficient thickness to last the entire etch. If the SiN mask is too thick, the thin resist for the grating process will spin non-uniformly and build up at the edges of the mask. After several calibrations it was determined that a SiN mask of 200 Å was sufficient for a grating etch depth of 500 Å, while still thin enough to avoid uniformity problems when spinning the resist. The SiN is deposited in PECVD and patterned using standard photolithography and SF_6 RIE etch.

After forming the SiN mask and cleaning the sample thoroughly, the resist for the grating process is applied and exposed as described above. The exposure and development is followed by a hard bake to harden the resist before the dry etch. Before the etch, the sample is also cleaned very briefly in O_2 plasma. This cleaning step is critical to obtain uniform, consistent gratings.

The gratings are etched in Methane/Hydrogen/Argon RIE. The process is a multi-step process, usually very reproducible if certain precautions are taken. First, the etch will slowly attack the photo resist mask, and eventually remove it completely. To minimize this effect, the first minute of the etch is done at low voltage, where the etch rate is very small and a layer of polymer is deposited on the photo resist.

This polymer layer serves to protect the photo resist when the etch voltage is increased. Secondly, the etch rate is dependent on loading effects. Near the edges of the sample, the etch rate is higher than at the center, furthermore the etch rate depends on how big a fraction of the sample surface is etched and how much is masked. With the devices in this work, most of the sample surface is masked, therefore the etch rate variation is minimal. To further reduce this problem, the chamber can be loaded with sacrificial InP wafers around the actual device sample [6]. With these precautions and by using the same sample size and loading conditions every time, the process was highly reproducible.

The gratings are slightly under-etched in the RIE etch; ideally the etch is stopped as close as possible to the InP stop etch layer without exposing it. After the dry etch, the sample is etched very briefly in H_2SO_4:H_2O_2:H_2O etch. This etch is selective, and will remove the remaining InGaAsP in the grating, but stop on the InP surface. The brief wet etch also removes crystal damage from the heavy Argon ions in the RIE etch [7]. This damage layer is very thin, but can contribute to waveguide propagation losses and reduced carrier lifetime, resulting in decreased tuning efficiency, particularly at low tuning currents. If the dry etch was over-etched, and the InP stop etch layer partly etched, the wet etch will not remove the etch damage. The grating process is concluded with a thorough clean to remove remaining polymer and photo resist. Finally the SiN mask is removed, and the

sample is prepared for MOCVD regrowth. Figure 3.5 shows a SEM picture of the etched grating.

Figure 3.5 *SEM picture of etched first-order DBR grating before regrowth*

3.4 Fabrication of grating quarterwave-shift

The far-field holographic method of grating fabrication described above does not allow for easy fabrication of quarterwave-shifted gratings, since the entire sample is exposed simultaneously with a continuous interference pattern. Complicated two-layer resist processes can be used with far-field holography to produce the phase-shift in the grating [8], but this is a difficult process with poor reproducibility. In particular, achieving uniformity in grating coupling coefficient (grating depth and duty cycle) over the entire sample is problematic. In this work a different approach was used, where the phase-shift is applied to the optical field instead of to the grating pattern.

In a ridge waveguide structure, the effective index of propagation depends on the width of the waveguide, shown in Figure 3.6 for the structure in "design 2".

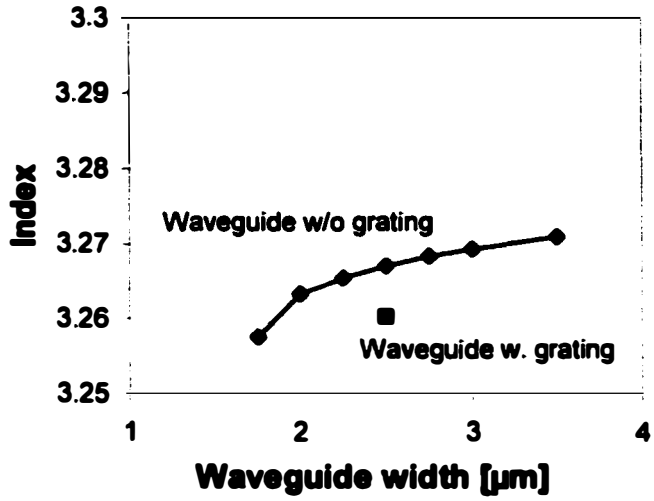

Figure 3.6 *Effective index vs. waveguide width for waveguide without grating. Also shown is the average effective index for the grating section*

By inserting a short length of waveguide with a different width between two sections of DBR grating, as illustrated in Figure 3.7, the optical field experiences a phase-shift relative to the grating phase. By proper design of the waveguide sections, a λ/4-shift can be obtained by satisfying the requirement:

$$L \cdot \Delta\beta = p\frac{\pi}{2} \Leftrightarrow L = p\frac{\lambda_0}{4\Delta\bar{n}}$$

where L is the length of waveguide between the two grating section, $\Delta\beta$ is the change in propagation constant, λ_0 is the free-space wavelength, $\Delta\bar{n}$ is the difference in effective index of propagation between the two waveguide widths, and p is an odd integer. With a waveguide width of 2.5μm in the grating sections, and 3μm in the phase-shift section, a quarterwave shift corresponds to a length of 41μm.

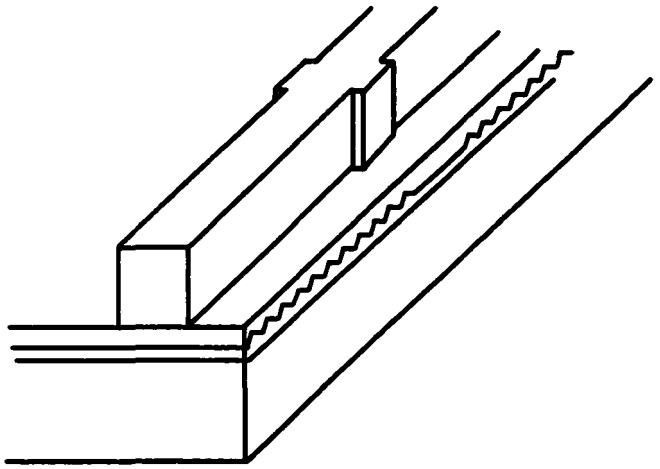

Figure 3.7 *Waveguide with phase section*

The described method for obtaining a phase-shift has an additional advantage. With a regular λ/4-shifted DBR grating, tuning takes place by injecting carriers in the entire grating length, thereby changing the index and shifting the filter characteristics including the notch exactly at resonance. With the approach used in this work, tuning can take place by injecting carriers in the phase section only,

shifting the position of the filter notch without changing the stopband position. This maximizes the usable spectrum and total channel count, and reduces the interference of the switching action on the express channels. At the same time, tuning the 41μm phase-section requires less current compared to tuning the entire 300μm grating. Since carrier injection causes not only a change in index, but also an increase in propagation loss, tuning the phase-shift section causes lower loss than tuning the entire grating. A final advantage is the possibility of including gain in the DBR sections to compensate for waveguide loss. This will be discussed in the Future Work section of Chapter 5.

3.5 Device processing

In section 3.3, the fabrication of DBR gratings was described. This section describes the device fabrication after the wafer has been regrown with p-cladding and contact layer on top of the gratings. The complete process flow is shown in Figure 3.8, and the complete recipe can be found in Appendix A.

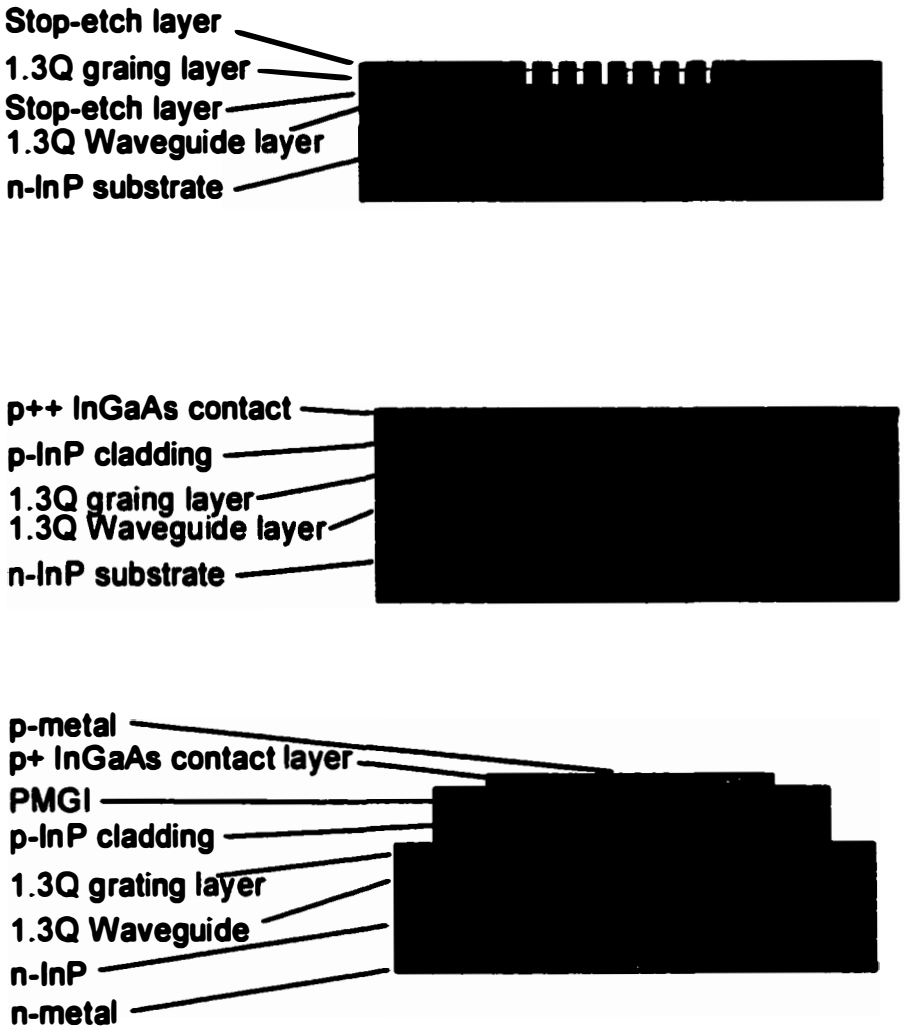

Figure 3.8 *Process outline for fabrication of filters and ADMs*

From the two material designs, filters and ADMs were fabricated. The filters consisted of straight waveguides with embedded λ/4-shifted DBR gratings. The ADMs had two first-order λ/4-shifted filters integrated with a directional coupler, as described in Chapter 2.

The first processing step following the regrowth is the definition and fabrication of the waveguides. For this step SiN was used as etch mask; the SiN was patterned using standard a standard photolithography process, and the photo resist pattern was transferred to the SiN by RIE SF_6 etch. In the first process runs, the SiN was etched in CF_4 plasma or RIE, but further characterization showed that the SF_6-chemistry yielded better definition, with cleaner lines in the longitudinal direction. This is important to minimize the scattering loss contribution to optical propagation losses. The SF_6 etch also gave a cleaner field surface after the etch.

Initially, the SiN mask was defined using regular contact photolithography. This approach was abandoned, and a 5:1 reduction stepper-aligner was used for the exposure instead. Besides improving reproducibility, the stepper aligner gave better waveguide definition, more controllable separation between the closely-spaced waveguide in the coupler section, and thanks to the improved resolution, the S-bends in the ADM devices were closer to the ideal smooth, curved shape. The device yield also improved significantly. Figure 3.9 shows a close up of the coupler section after the waveguides have been etched.

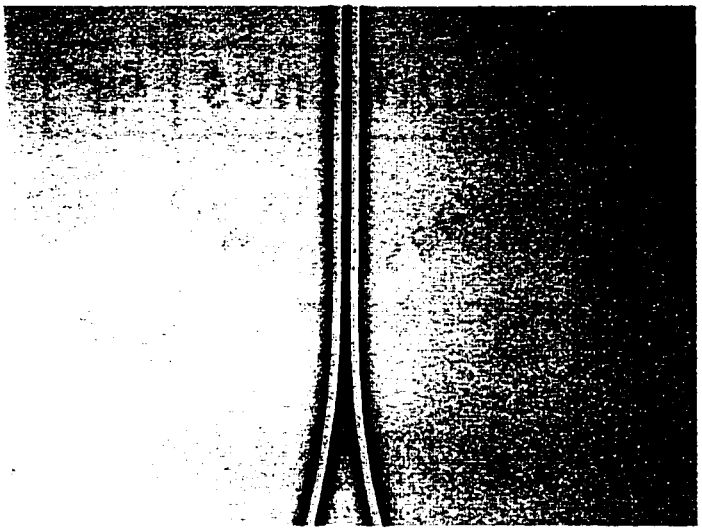

Figure 3.9 *Close-up micrograph of etched waveguides in coupler section of ADM device.*

Using the SiN as etch mask, the waveguides were etched with a combination of wet and dry (RIE) etch. Using in-situ monitoring, Methane-Hydrogen-Argon RIE was used to etch through the top contact layer and the InP p-cladding, stopping approximately 1000 Å before the InGaAsP waveguide layer. A quick wet etch in HCl removed the remaining InP and also served to clean up etch damage from the heavy Ar-ions.

Between the waveguides in the coupler, spaced 1 μm apart, the dry RIE etch profile is rough and non-uniform. Due to transport effects in the narrow gap, the sidewalls curve out, changing the coupling between the waveguides in an uncontrollable way. The HCl-etch removed this as well, to obtain nearly vertical sidewalls. At the

same time, it is essential to keep the final HCl-etch to a minimum to maintain smooth sidewalls in the S-bend sections. Stopping the RIE etch 1000 Å before the waveguide and following this with 15 seconds etch in HCl proved to be the best compromise between the two concerns. Longer wet etches caused a significant degradation of the waveguide quality in the curved sections by exposing crystallographic planes, in addition to a decrease of waveguide width [9].

Following the etch of the waveguides, the SiN mask was removed in HF. The sample was planarized using a multilayer PMGI process. Several layers of PMGI were spun, curing each layer before spinning the next. At a total thickness of ~4μm, the waveguides were completely buried in PMGI and the sample planarized. The PMGI was etched back until the tops of the waveguides were exposed. This could be done either by flood exposing and developing the PMGI repeatedly or by etching the PMGI in O_2 RIE. The former approach was chosen for its simplicity, and to minimize the amount of plasma damage to the top InGaAs contact layer.

Top Ti/Pt/Au p-contacts were deposited and patterned using a lift-off process, then annealed. Electrical isolation between contacts was achieved by a shallow dry etch between the contacts. By etching through the p+ InGaAs layer and approximately 4000 Å of the p-cladding, an isolation of > 1kΩ was obtained, while the etch was shallow enough to cause minimal perturbation to the optical mode. The wafer was thinned to 100μm thickness and a Ni/AuGe/Ni/Au n-contact was deposited and

annealed. Figure 3.10 shows micrographs of the filter section and the curved waveguide transition from the coupler to the filter.

Figure 3.10 *Micrographs of filter section (left) with separate contacts for tuning of the DBR sections and the l/4-phase section, and the curved waveguide transition (right) between the filter and the coupler.*

After cleaving and screening, the best bars of devices were anti-reflection coated for further testing. The results are presented in Chapter 4.

3.6 Tunability

This section deals with the current tunability of the filters and add-drop multiplexers. Injection of carriers in the waveguide layer will cause a change in the refractive index of the material through the plasma loading effect. Here a phenomenological description of the index change as a function of carrier density

will be used [10, 11]. The model assumes linear relationship between carrier density change and index change, a reasonable assumption at low carrier densities. Using the linear model, the index change is given as:

$$\Delta n = \Gamma \frac{dn}{dN} \Delta N$$

where Δn is the change in index, Γ is the confinement factor and dn/dN is the slope of index change versus carrier density change. For the purpose of this section, an empirical value of -10^{-20} cm^3 is used. In the case of non-uniform carrier density, the expression above can be generalized to:

$$\Delta n = \frac{dn}{dN} \frac{1}{d} \int E(x) \Delta N(x) dx$$

where d is the waveguide thickness, E(x) is the normalized optical field magnitude, and $\Delta N(x)$ is the local change in carrier density. The integration is over the entire optical mode profile in the transverse direction. Lateral variations have been neglected. The local change in carrier density $\Delta N(x)$ as a function of current can be calculated from the standard transport and continuity equations [10]. For the calculations here the "SimWindows" application was used to determine band diagrams and carrier densities at different bias levels. The normalized optical field profile was calculated using a 1-D mode solver. Figure 3.11 shows the band diagram at 10mA current in the 41μm long phase shift section. The carrier density is plotted in Figure 3.12.

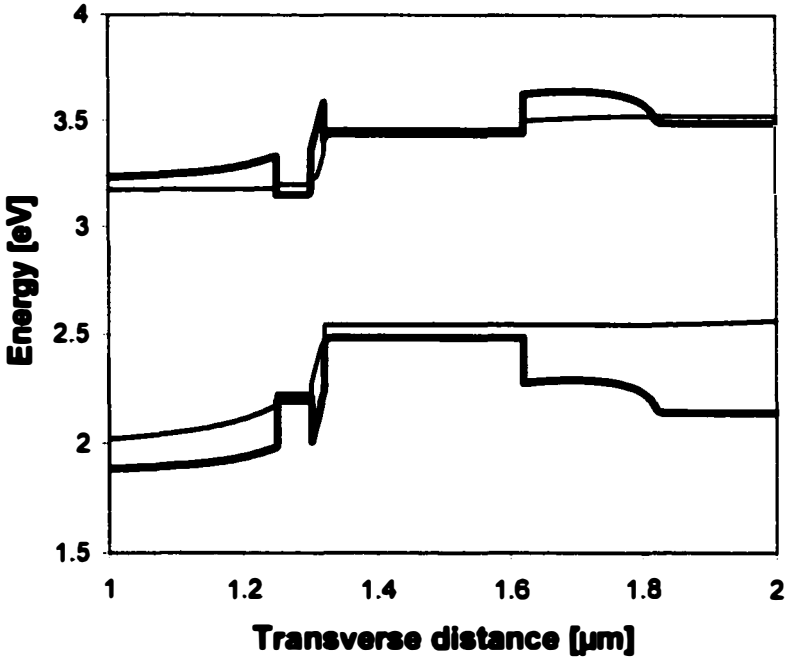

Figure 3.11 *Band diagram in the phase section for 10 mA bias current. The heavy lines are the conduction and valence bands. The thin lines the quasi-fermi levels for electrons and holes.*

From the change in index, the wavelength shift can easily be calculated as:

$$\Delta\lambda = \lambda \frac{\Delta n}{n}$$

Combining the carrier density calculations with the mode profile, and using the equations above, the wavelength shift of the resonance notch can be calculated. The result is shown in Figure 3.13, predicting a wavelength shift of 8 nm at 10mA

bias current, assuming 100% injection efficiency. This is compared to the ideal case with uniform carrier density in the waveguide and grating layers, where the shift is ~10 nm at 10 mA bias current.

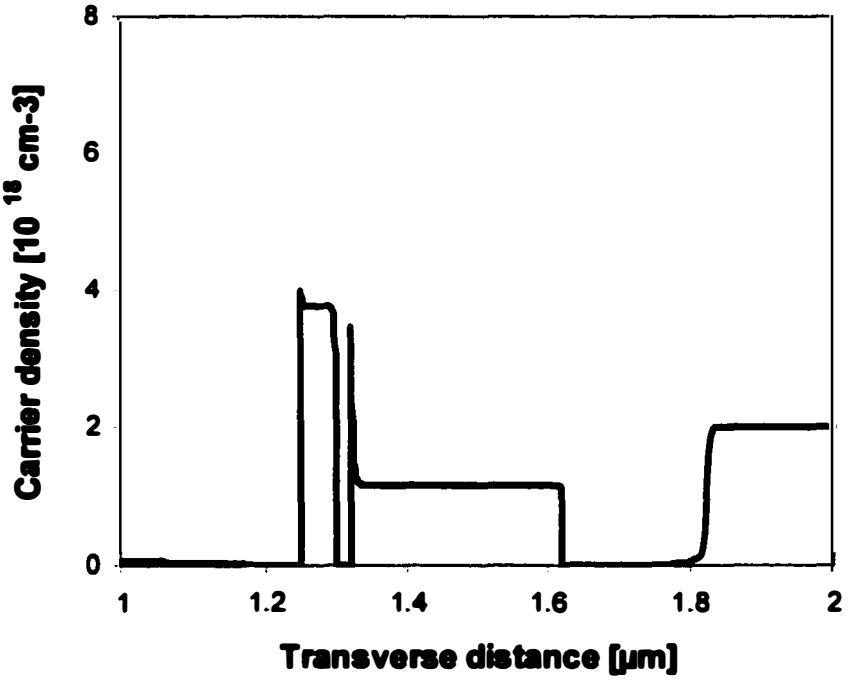

Figure 3.12 *Electron density in phase section at 10 mA bias current*

The small difference between the wavelength shift assuming uniform carrier distribution and the shift in the design described here, indicates that the effect of the hole barrier formed by the InP stop etch layer is minor.

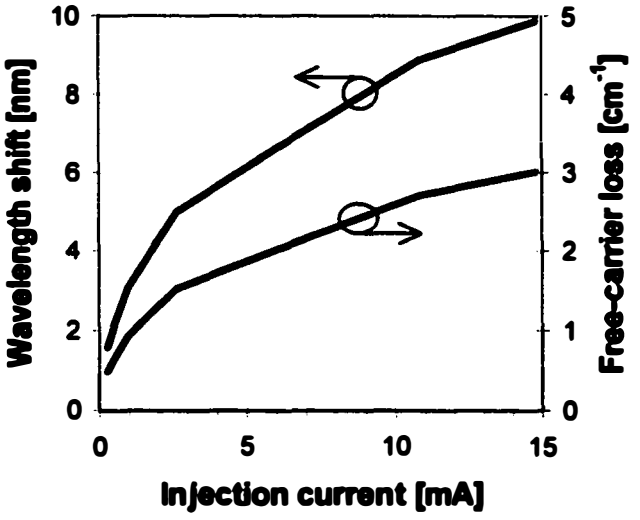

Figure 3.13 *Theoretical device response to current tuning. Figure shows wavelength shift and free-carrier absorption loss vs. injection current in the phase section*

Two important effects have been neglected so far. First, the current injection will cause an increase in device temperature through Joule heating. The temperature increase in turn causes a shift to longer wavelength, counter-acting the shift caused by plasma loading. In Chapter 4 this effect is clearly visible in the experimental results. Secondly, the injected carriers cause not only a change in index, but also increases the optical losses through free-carrier absorption. Using a classical Drude-model for loss due to free-carrier absorption, the calculation of local carrier density and mode profile was used to calculate the increase in optical losses. The

results are also shown in Figure 3.13. In Chapter 2 the importance of minimizing losses was discussed, and as the result in the figure demonstrate, the tuning range will be limited by the increase in loss to 4 nm in the ideal case neglecting thermal effects and assuming a first-order filter with maximum acceptable loss of $1.5cm^{-1}$. Chapter 4 contains experimental results investigating the available tuning range.

3.7 Summary

Chapter 3 covered the device design and fabrication, starting with waveguide design and device implementation of the filter designs obtained in Chapter 2. Two different structures were described, and their respective advantages and disadvantages were discussed. Experimental results will be presented in Chapter 4. One important fabrication issue was the implementation of a λ/4-shifted DBR grating. The far-field holographic method used for grating fabrication is not suitable for fabrication of conventional λ/4-shifted DBR, instead a design based on an alternative approach was shown. Besides overcoming the limitation of the far-field holographic exposure method, the proposed phase-shift waveguide implementation had an advantage in terms of device tunability. This was the topic of the last section, where the expected tuning range was calculated, and the tuning range limits were discussed. The calculations yielded a predicted tuning range of 8 nm, assuming 100% injection efficiency.

The chapter also described in some detail the device fabrication process, with particular focus on the critical steps with significant impact on device performance.

References

[1] L. A. Coldren and S. W. Corzine, *Diode Lasers and Photonic Integrated Circuits*. New York: John Wiley & Sons, Inc., 1995.

[2] M. Heinbach, M. Schienle, A. Schmid, B. Acklin, and G. Müller, "Low-Loss Bent Connections for Optical Switches," *IEEE Journal of Lightwave Technology*, vol. 15, pp. 833-7, 1997.

[3] D. M. Tennant, T. L. Koch, J.-M. Verdiell, K. Feder, R. P. Gnall, U. Koren, M. G. Young, B. I. Miller, M. A. Newkirk, and B. Tell, "Multiwavelength distributed Bragg reflector laser array fabricated using near field holographic printing with an electron-beam generated phase grating mask," *Journal of Vacuum Science & Technology B (Microelectronics and Phenomena)*, vol. 11, pp. 2509-13, 1993.

[4] P. I. Jensen and A. Sudbø, "Bragg Gratings for 1.55-μm Wavelength Fabricated on Semiconductor Material by Grating-Period Doubling Using a Phase Mask," *IEEE Photonics Technology Letters*, vol. 7, pp. 783-5, 1995.

[5] V. Jayaraman, "Extended tuning range semiconductor lasers with sampled gratings," in *Dept. of Electrical and Computer Engineering*. Santa Barbara, CA: University of California, Santa Barbara, 1994, pp. 200.

[6] K. Janiak and U. Niggebrügge, "Investigation of macroscopic uniformity during CH_4/H_2 reactive ion etching of InP and improvement using a guard ring," presented at IPRM 1996. Eighth International Conference on Indium Phosphide and Related Materials, Schwabisch-Gmund, Germany, 1996.

[7] T. Bottner, H. Krautle, E. Kuphal, K. Miethe, and H. L. Hartnagel, "Surface- and sidewall-damage of InP-based optoelectronic devices during reactive ion etching using CH_4/H_2," presented at IPRM 1996. Eighth International Conference on Indium Phosphide and Related Materials, Schwabisch-Gmund, Germany, 1996.

[8] K. Utaka, S. Akiba, K. Sakai, and Y. Matsushima, "λ/4-shifted InGaAsP/InP DFB lasers by simultaneous holographic exposure of positive and negative photoresists," *Electronics Letters*, vol. 20, pp. 1008-9, 1984.

[9] M. Seto, R. J. Deri, A. Yi-Yan, E. Colas, W. J. Tomlinson, R. Bhat, and A. Shahar, "Fabrication of Submillimeter-Radius Optical Waveguide Bends with Anisotropic and Isotropic Wet Chemical Etchants," *IEEE Journal of Lightwave Technology*, vol. 8, pp. 264-70, 1990.

[10] J. P. Weber, "Optimization of the Carrier-Induced Effective Index Change in InGaAsP Waveguides - Applications to Tunable Bragg Filters," *IEEE Journal of Quantum Electronics*, vol. 30, pp. 1801-16, 1994.

[11] B. R. Bennett, R. A. Soref, and J. A. del Alamo, "Carrier-Induced Change in Refractive Index of InP, GaAs, and InGaAsP," *IEEE Journal of Quantum Electronics*, vol. 26, pp. 113-22, 1990.

Chapter 4 Device characterization

4.1 Introduction

This chapter contains the results of the characterization of the narrow band filters and add-drop multiplexers (ADMs). The characterization focuses on the static device performance and extraction of the parameters that were used to specify the design. Deviations from the response expected from theory will be discussed, and suggestions to improvements will be given. Some of these suggestions will be further expanded in the section on future work in Chapter 5.

The first section of the chapter covers waveguide characterization and the measurements on simple first-order notch filters. From the measured data, waveguide and filter parameters are extracted. The section also covers the tuning capabilities.

The following section deals with the integrated ADMs consisting of directional couplers integrated with narrow band filters. As it will be seen, the performance of these devices was insufficient to obtain good low-noise measurements. A discussion of the problems and proposed solutions will be given. Finally, the chapter is concluded with a summary section.

4.2 Filter characterization

The goal of this work is implementation of InP waveguide based integrated add-drop multiplexers, but for characterization purposes filters without couplers were also designed and fabricated. In addition to that, regular waveguides without filters were included to obtain information about the process and regrowth quality. This section covers the characterization of the filters and waveguides. The measurements are done using a HP tunable laser and a calibrated detector as shown in Figure 4.1. The laser has a resolution of 0.1nm (=12.5 GHz at 1.55 μm wavelength). The signal from the laser is coupled through a polarization controller to the waveguide using a lensed single mode fiber. On the output side, the signal is collected with another lensed SM fiber. For the purpose of alignment and monitoring the mode shape, the fiber on the output side can be replaced by a microscope lens imaging the facet onto a CCD camera. A computer controls the tunable laser and the power meter for collection of data during wavelength scans.

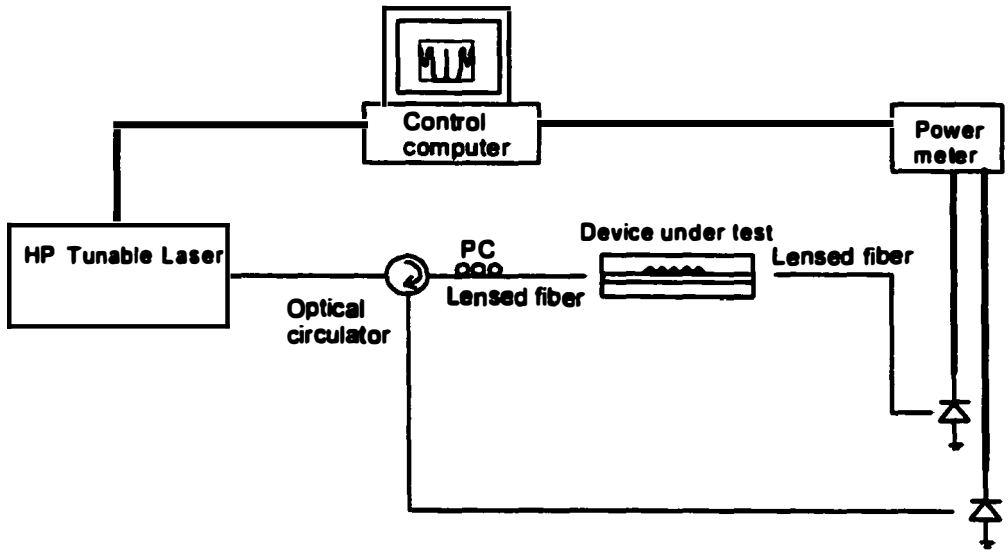

Figure 4.1 *Measurement set-up for filter and add-drop multiplexer characterization*

Since no attempt was made at designing a polarization independent device, all results presented here are for TE polarization. For applications in a communication system, polarization independence is imperative, and future work should include design improvements to achieve this. Chapter 5 will include a discussion about this topic.

The device results in this section were from bars cleaved at approximately 550-μm length, with two DBR gratings separated by a 41-μm phase-shift section. For comparison, filters without the λ/4 shift were also characterized. In both cases the fiber-to-fiber loss was measured to be 22 dB or worse. To identify the cause of the losses, transmission through 800 μm long waveguides without gratings and anti-reflection coatings was measured, shown in Figure 4.2.

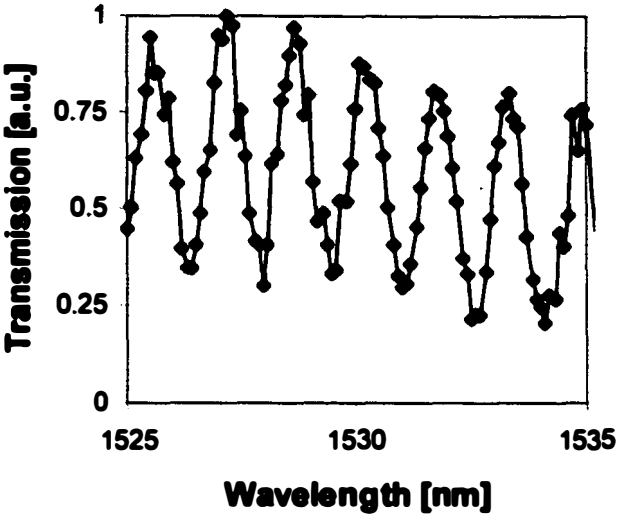

Figure 4.2 *Transmission through uncoated 800-μm waveguide Fabry-Perot cavity.*

The waveguide propagation loss α_i, can be calculated from the measurements of the modulation resonances of the Fabry-Perot resonances:

$$\alpha_r = \alpha_i + \frac{1}{L}\ln\left(\frac{1}{R}\right)$$

$$F = \frac{\pi \exp(-\alpha_r L/2)}{1-\exp(-\alpha_r L)}$$

$$\frac{I_{max}}{I_{min}} = 1 + \left(\frac{2F}{\pi}\right)^2$$

where α_r is the effective distributed loss coefficient, α_i is the internal propagation loss coefficient, R is the facet power reflectivity, L is the cavity length, F is the

cavity finesse, and I_{max} and I_{min} are the peak transmission, respectively. Figure 4.3 shows the modulation depth vs. propagation loss coefficient, for an uncoated FP cavity length of 800μm.

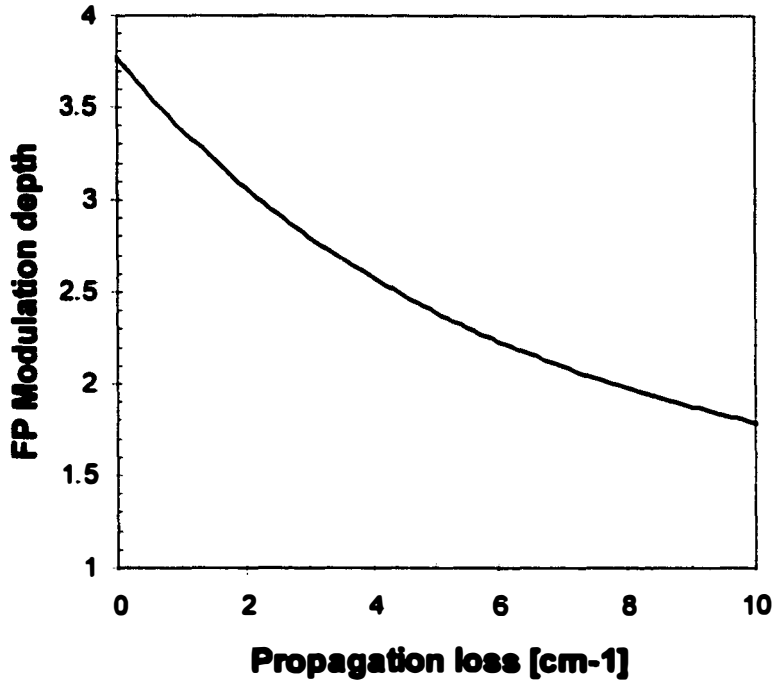

Figure 4.3 *Fabry-Perot modulation depth as function of internal propagation loss coefficient for a 800μm long uncoated waveguide*

The measured modulation depth (I_{max}/I_{min}) is approximately 3.1, corresponding to a propagation loss of 1.9 cm^{-1}. This waveguide had no grating, but was otherwise identical in process and structure to the DBR filter devices. In the uniform waveguide, the regrowth was InP on an InP surface; in the waveguide with grating, the horizontal surfaces in the grating are InP while the vertical sidewalls have

exposed InGaAsP. This difference is likely to cause higher losses in the DBR sections. Etch damage and scattering in the gratings also contribute to the propagation losses. With these qualifications in mind, the result shows that the design and fabrication of a low loss waveguide structure has been successful. In the discussion of the filter measurement results, the loss coefficient for the waveguides with grating is extracted from measurements.

The results discussed above were obtained with the structure labeled as 'design 2' in Chapter 3. The initial runs with design 1 had higher loss, best case was ~12 cm^{-1} waveguide loss in waveguides without grating. In the filters, the losses were much higher, and it was impossible to get good quantitative measurements of the filter characteristics. As described in Chapter 3, in 'design 1' the regrowth was InP directly on the InGaAsP waveguide, both in the grating sections and in the uniform waveguides. The high loss is most likely due to poor material quality at the regrowth interface. All the results below were obtained with the 'design 2' structure with separate grating layer.

Based on the value for waveguide loss, the 22 dB fiber-to-fiber loss can be attributed to coupling losses between the waveguide and fibers. For a practical device in a communication system, this value of fiber-to-fiber loss is clearly excessive and should be reduced. Substantial improvement can be achieved with integrated mode converters.

Unfortunately, the high coupling loss between fiber and device also makes measurements complicated. For the purpose of filter characteristics, it is desirable

to measure both reflection and transmission, and in that way determine the device performance in terms of both the express channels and the drop channel. With a return loss of at least 22 dB, the reflected signal from the device is very weak, and on the same order of magnitude as reflections from imperfect facet coating and spurious reflections in the measurement set-up. Consequently, the measured reflected signal becomes a superposition of the device reflection signal and the spurious signals. The interference of these signals depends on optical path lengths in the fibers, which in turn vary due to temperature effects and mechanical instability. All the reflection measurements were very noise and showed unstable interference patterns, making reproducible measurements impossible.

Figure 4.4 shows the device schematic of the filters characterized in this section. The device had two 150 μm long DBR sections separated by a 41-μm long phase section. The filter had approximately 100 μm of passive waveguide on each side, bringing the total device length to 550 μm. Measurements were done at room temperature (20°C) on a temperature-controlled stage.

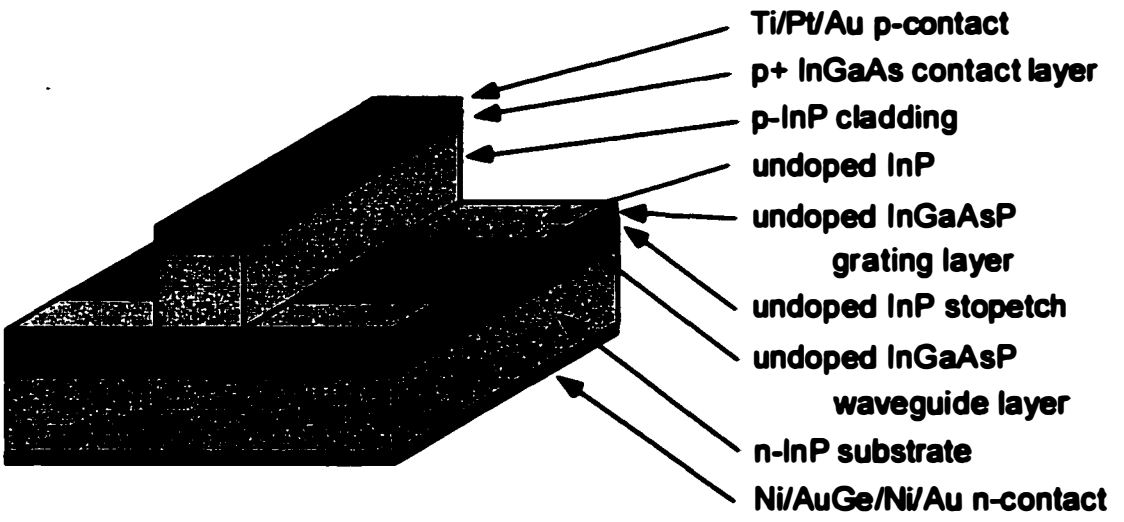

Figure 4.4 *Filter device structure*

Figure 4.5 shows the measured transmission for the λ/4-shifted filter. The center wavelength is at 1532.2 nm, instead of the 1550 nm it was designed for. The cavity resonance is also shifted to a shorter wavelength. The shift is partly due to the fact that the waveguide layer was thinner than designed. This also explains the small misalignment of the λ/4-cavity resonance from the center of the stop band.

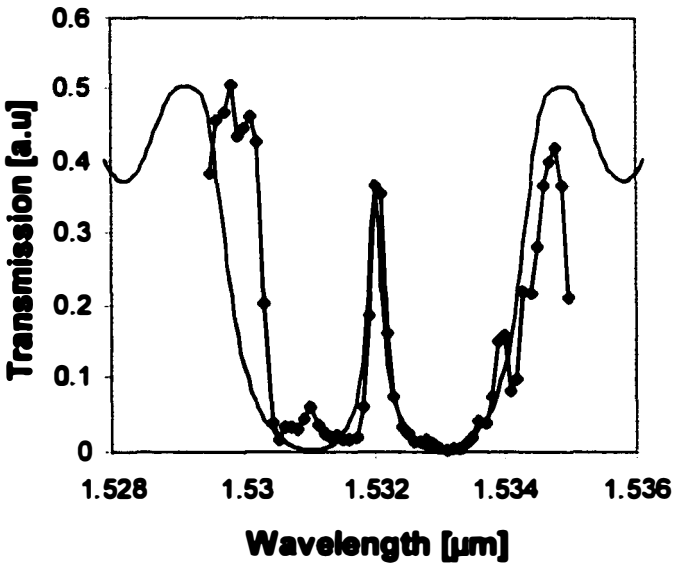

Figure 4.6 *Measured (-•-) and calculated (-) transmission of λ/4-shifted DBR filter. Calculated response is based on extracted device parameters for resonance wavelength and grating coupling coefficient, and waveguide propagation loss as fitting parameter.*

The stop band bandwidth is measured to 3.7 nm, compared to the design value of 4.0 nm. The measured value corresponds to a grating coupling coefficient of 130 cm^{-1}. The notch bandwidth is 38 GHz (0.3 nm), and the relative transmission at resonance is –1.5dB. The design goals were 15 GHz and full transmission, respectively. The isolation between reflected and transmitted channels is 13 dB. For comparison, similar InP DBR-based devices in the literature have achieved 0.7nm and ~10dB isolation [1], 7nm bandwidth and 11dB isolation [2], and 2nm

bandwidth and 18dB isolation [3]. An apodized SiO_2-SiO-based device structure similar to the one described in this work, achieved 1.5nm bandwidth and 30dB isolation [4]. As mentioned in Chapter 1, the best result obtained from a InP DBR-grating based add-drop device is 0.4nm bandwidth and >20dB cross-talk isolation [5]. This device was based on a grating-assisted vertical coupler and tunable by heating with a Cr thin-film heater.

The deviations from design targets in notch bandwidth and transmission can be explained by the propagation loss in the waveguide, which causes a decrease in the filter-Q, as discussed in Chapter 2. Figure 4.6 also shows a calculated response, using the correct center wavelength and coupling coefficient, and using waveguide loss as fitting parameter. The best fit is obtained with a loss value of 5 cm^{-1}. Compared to the loss in a regular waveguide without gratings, the DBR grating has additional 3 cm^{-1} loss.

The filter wavelength can be tuned by temperature. Figure 4.7 shows the notch wavelength as a function of the substrate temperature. The tuning rate is 0.12 nm/°C over 5.4 nm. No significant degradation of the filter characteristic was observed over this tuning range. The measurement of the tuning range was limited by the capability of the temperature-controlled stage.

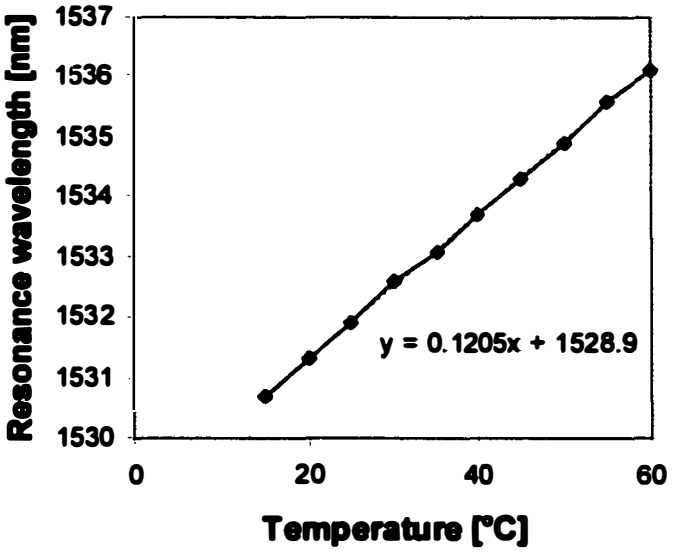

Figure 4.7 *Temperature tuning of λ/4-shifted filter.*

In the introduction, the ability to tune the filters and ADMs by current injection was mentioned as an important advantage of implementing the devices using semiconductor technology. For that purpose the filters were designed and fabricated with electrical contacts for current injection, and the resonance wavelength was measured as a function of injection current. Figure 4.8 shows the shift in wavelength with increasing current. A tuning range of 2.2 nm (275 GHz) was achieved with a bias current of 4 mA, corresponding to a current density of 3kA/cm^2. The 275 GHz tuning range is more than sufficient for switching between two channels spaced by 100 GHz.

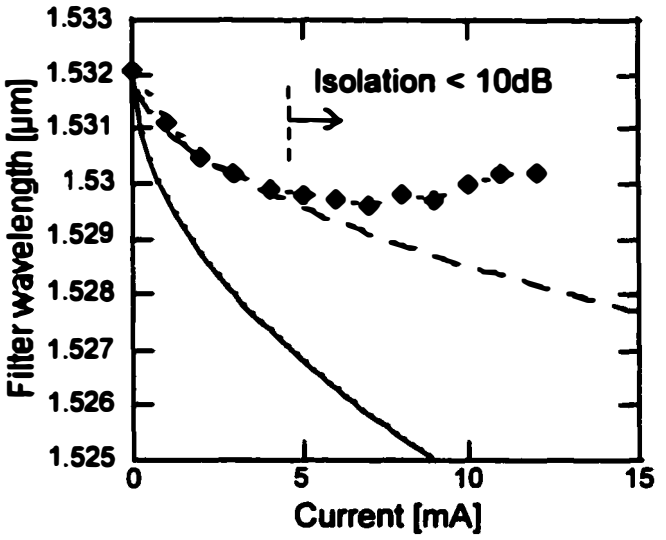

Figure 4.8. *Resonance wavelength vs. bias current for λ/4-shifted DBR filter. Diamonds show measured response, the full and the dashed lines are theoretical characteristics for 100% and 20% injection efficiency, respectively. Heating effects have been neglected in the theoretical results.*

Because injected carriers not only change the index of the semiconductor material, but also contribute to waveguide propagation loss, the tuning range is limited by deterioration of the filter response with increasing loss. Figure 4.9 shows the filter transmission response at 5 mA current. The isolation has decreased to ~9dB, and the pass-band notch bandwidth has broadened to 0.9nm.

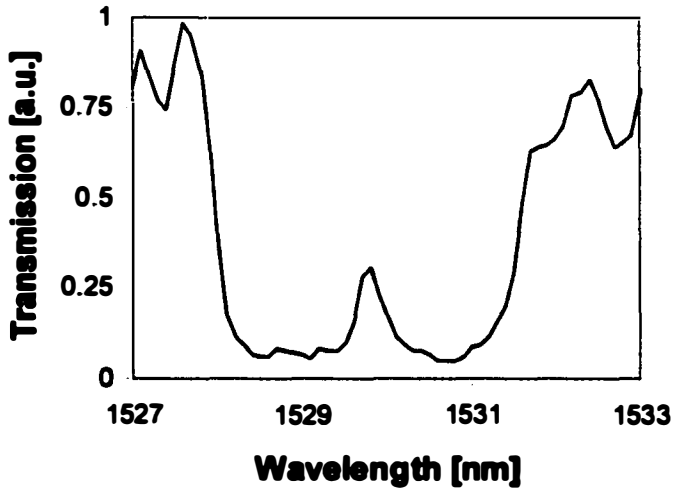

Figure 4.9 *Filter transmission characteristics at 5 mA current.*

Besides the increase in loss, the tuning range is also limited by the temperature increase due to Joule heating. As seen above in the temperature tuning experiment, an increase in temperature causes a shift to longer wavelength, the opposite direction of the shift from carrier injection. At higher current densities, the heating effects dominate, and cancel the shift from plasma loading. Increasing the available tuning range can be done by reducing the heating effects, most efficiently by changing the design to minimize the diode resistance, and the thereby reduce the Joule heating. Increasing the doping level in the p-ridge or reducing the doping offset layer thickness can achieve this. As discussed in Chapter 3, this is a trade-off with the goal of maintaining a low-loss waveguide. One solution would be to base the design on the higher order Chebyshev or Butterworth filters, which are

less sensitive to waveguide loss. This would allow for a reduced doping offset layer thickness, and an increased tuning range.

Device design with better heat properties would also help to alleviate the problem, e.g. buried structures with lower thermal resistance. Finally, higher injection efficiency can increase the wavelength shift for a given tuning current. The injection efficiency can be improved by using lower band gap material in the waveguide [6, 7], again at the expense of increased propagation loss. More significant is the improvement in tuning efficiency of lower bandgap material. As an example, the tuning efficiency of 1.4 μm bandgap wavelength is 50% higher than that of 1.3 μm bandgap wavelength material for a signal wavelength of 1.55 μm [6].

4.3 Add-drop multiplexer characterization

Having covered the experimental characterization of waveguides and filters in the previous section, attention is now turned to the measurements on the integrated Add-Drop Multiplexers. The measurement set-up and procedures are similar to those described in Section 4.2 and Figure 4.1.

During the measurements on the ADMs several problems became apparent. Some were related to the measurements, some were device problems. The measurement problems will be discussed first.

As with the filters, the coupling losses were very high at ~13 dB/facet. The total device loss was ~10dB. Consequently, at –36dB, the output signal was relatively weak, and signal to noise ratio for all the measurements was poor. The problem of interference between spurious reflections in the set-up and the device signal was also present in these measurements, further complicating the characterization. Finally, light transmitted through the substrate made measurements on the bar output particularly difficult.

Turning to device issues, most important was the response of the directional coupler part of the device. The coupler was designed for 100% coupling at 1.55μm, but the measured devices had about 65% coupling to the bar output, and 35% to the cross port. This is believed to be due to fabrication tolerances: Waveguide thickness and ridge width/spacing.

Despite the problems with measurement noise and the coupler, the wavelength selectivity of the embedded filters was characterized. Figure 4.10 shows the output from the integrated coupler and filter at different wavelengths, as captured with an IR camera.

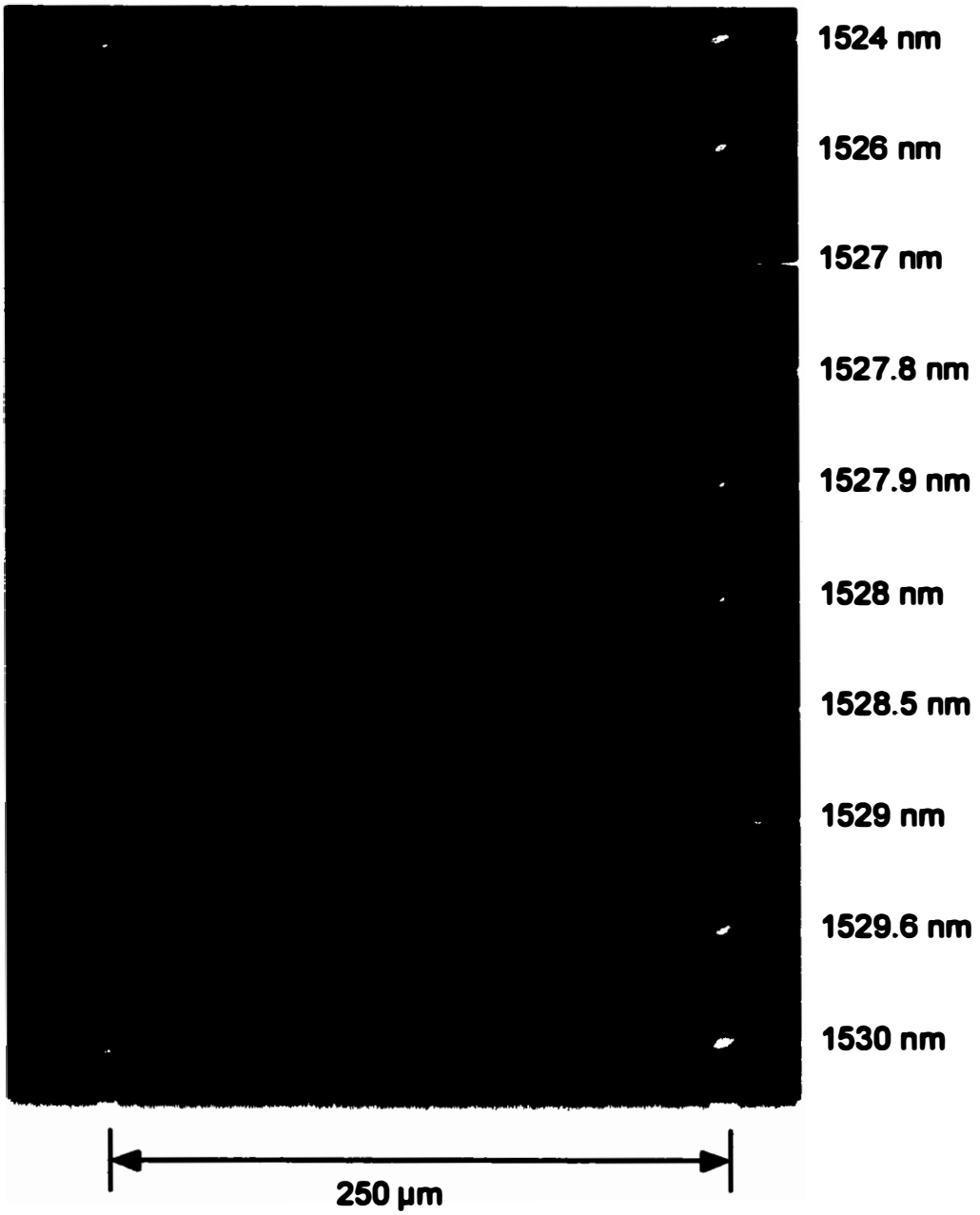

Figure 4.10 *Output from ADM captured with an IR camera. The cross port is to the left, bar to the right.*

A couple of observations can be made from the measurements in Figure 4.10. First, the pictures clearly illustrate the problem of spurious light at the bar port. However, the measurement qualitatively shows the function of the device. At 1526nm and 1530nm light is passed through, and between these wavelengths light is reflected. At the center of this band, at 1527.9 nm a narrow pass band can be observed. This was quantified by measuring the output from the cross port, shown in Figure 4.11.

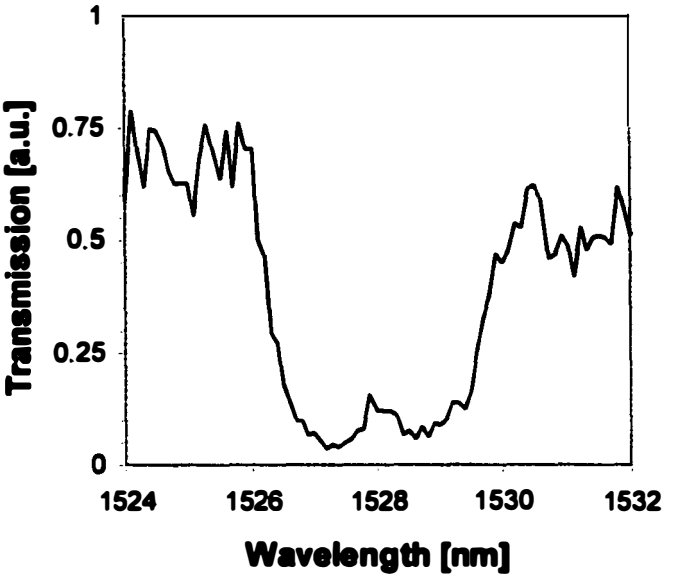

Figure 4.11 *Measured transmission from input to cross port.*

Compared to the filters measured in previous section, the stop band in the ADM is narrower, and the notch is wider and shallower. This can be due to higher

waveguide loss in the filter sections. The resonance wavelength is also shifted to a slightly shorter wavelength. Material non-uniformity and variations in waveguide width across the wafer can explain this. The fact that both the resonance wavelength and coupling between the waveguides were substantially different from the design value, points to problems with process control in the add-drop devices. The higher loss in the add-drops compared to the linear filters also point in that direction.

4.4 Summary

In this chapter the experimental results for the narrow band notch filters and integrated Add-Drop Multiplexers were presented. Notch bandwidth of 0.3 nm (38 GHz) and isolation of 13 dB were achieved with the filters. Bandwidth and isolation were both limited by waveguide propagation loss. The loss parameters derived from measurements were 2 cm^{-1} and 5 cm^{-1} in the sections without and with DBR grating, respectively. Both temperature and current tuning were characterized. With temperature tuning a tuning rate of 0.12 nm/°C over 5.4 nm was achieved. The measured tuning range was limited by the temperature control capabilities of the measurement set-up. With a waveguide band gap wavelength of 1.3 μm, the band gap shrinkage due to the increased temperature will cause only a very small increase in waveguide losses. This should make the tuning range substantially larger than the 5.4 nm measured here.

The current tuning range was 2.2 nm, at 4 mA current injection. The tuning range was limited by increased waveguide losses due to free-carrier absorption, at 4 mA the isolation had deteriorated to <10dB, and rapidly decreasing with increasing current. Another limit is the heating effect, limiting the wavelength shift to 2.7 nm is this structure.

The chapter also covered the characterization of the integrated ADMs. Several problems, both measurements problems and device issues, made a complete characterization impossible. First of all, the coupling length was not as designed. The filter part of the ADMs exhibited the right response qualitatively, but due to excess waveguide loss, the notch in the stop band is too broad and very shallow.

References

[1] R. C. Alferness, L. L. Buhl, M. J. R. Martyak, M. D. Divino, C. H. Joyner, and A. G. Dentai, "Narrowband GaInAsP/InP waveguide grating-folded directional coupler multiplexer/demultiplexer," *Electronics Letters*, vol. 24, pp. 150-1, 1988.

[2] Y. Shibata, S. Oku, Y. Kondo, T. Tamamura, and M. Naganuma, "Semiconductor Monolithic Wavelength Selective Router using a Grating Switch Integrated with a Directional Coupler," *IEEE Journal of Lightwave Technology*, vol. 14, pp. 1027-32, 1996.

[3] J. P. Weber, B. Stoltz, H. Sano, M. Dasler, O. Oberg, and J. Walz, "An integratable polarization-independent tunable filter for WDM systems: the multigrating filter," *Journal of Lightwave Technology*, vol. 14, pp. 2719-35, 1996.

[4] D. Mechin, P. Grosso, and D. Bose, "Add-Drop Multiplexer with UV-Written Bragg Gratings and Directional Coupler in SiO2-Si Integrated Waveguides," *IEEE Journal of Lightwave Technology*, vol. 19, pp. 1282-6, 2001.

[5] M. Horita, S. Tanaka, and Y. Matsushima, "Wavelength tunable optical add and drop multiplexer utilising coupled semiconductor waveguides and a striped thin-film heater," *Electronics Letters*, vol. 34, pp. 2240-1, 1998.

[6] J. P. Weber, "Optimization of the Carrier-Induced Effective Index Change in InGaAsP Waveguides - Applications to Tunable Bragg Filters," *IEEE Journal of Quantum Electronics*, vol. 30, pp. 1801-16, 1994.

[7] B. R. Bennett, R. A. Soref, and J. A. del Alamo, "Carrier-Induced Change in Refractive Index of InP, GaAs, and InGaAsP," *IEEE Journal of Quantum Electronics*, vol. 26, pp. 113-22, 1990.

Chapter 5 Summary and future work

5.1 Summary

The previous three chapters covered design, fabrication and characterization of quarterwave-shifted DBR filters and optical add-drop multiplexers based on integrated filters and horizontal directional couplers. In this chapter the results are summarized and suggestions for future improvements and development are discussed.

Chapter 1 of this work discussed the applications for a reconfigurable optical add-drop module, and compared a range of technologies and architectures available to achieve the required functionality. In terms of static filter performance, the glass-based arrayed waveguide gratings are at the present clearly superior to competing technologies, but with the disadvantages of large size, slow reconfiguration time and unsuitability for integration with active semiconductor devices. The proposed InP based device described in this work, or variations hereof, addresses all three of these concerns. The challenge for a DBR-filter based semiconductor device is achieving sufficiently narrow filter bandwidth under all operating conditions. As described in Chapter 2, this requirement precludes a filter based on a simple one-section DBR grating — the device parameters necessary to achieve the narrow filter bandwidth are impractical, and the sensitivity to loss makes current tuning impossible.

Instead, the design of first- and higher-order λ/4-shifted DBR filters was proposed. The first-order filters are indeed able to achieve the narrow bandwidth required, but the filter shape is not appropriate for the applications, and the maximum tolerable value of waveguide loss severely limits the tuning range. In this aspect, the higher-order filters, based on Butterworth or Chebyshev filter shapes, show more promise. A fifth-order Butterworth filter can be designed with >30dB cross-talk and 25GHz bandwidth, and with small sensitivity to waveguide propagation loss. It should be noted, that even though it may be possible to fabricate filters with extremely low loss, an increase in loss is inherent to tuning by current injection. This makes the robustness against propagation loss imperative, even for designs implemented in structures with low loss in the untuned state.

In addition to the improved tolerance to loss, the higher-order filters have a filter response shape more suitable for applications in communication systems. The pass-band, selecting the 'drop'-channel, is wide enough to support variations in signal wavelength or small changes in device characteristics, e.g. due to environmental changes. The 25 GHz pass-band filter mentioned above, will maintain >30dB isolation over 20GHz.

One significant limitation of the λ/4-shifted filters, both first- and higher-order versions, is the limit in total number of channels the filter can support. The total wavelength span of all channels cannot be wider than the width of the DBR stopband; in the designs covered in this work this width is ~800 GHz. More aggressive designs of higher-order filters are capable of covering at least 1200

GHz, still much too narrow for most applications. The next section will outline suggestions for improvements or extensions to accommodate a substantially larger wavelength span.

The section on device fabrication covered the critical design decisions and process steps necessary to obtain low-loss waveguides and reproducible gratings. The limitations to the far-field holography method for grating fabrication were circumvented by using a long phase section to apply the quarterwave shift to the optical field. The separate phase section also makes it possible to tune the notch filter while leaving the DBR stop-band virtually unchanged.

The results obtained from the first-order filters, presented in Chapter 4, were somewhat disappointing. Design 1, with no separate grating layer and regrowth directly on the InGaAsP waveguide, had high waveguide loss, to the extent that the narrow-band notch was virtually gone. In addition, the total fiber-to-fiber loss was too high to make good quantitative measurements.

The devices made from Design 2 epi, with a separate grating layer and InP stop-etch layer proved far better. A filter bandwidth of ~38GHz was obtained, with ~13 dB cross-talk isolation. Using the waveguide loss as fitting parameter, good agreement between calculations and measurements was achieved with a loss parameter of $\alpha = \sim 5 cm^{-1}$. As shown in Chapter 2, this value should be reduced to $<1.5\ cm^{-1}$ to achieve 20 dB cross-talk isolation in a first-order filter. Both temperature and current tuning were demonstrated. For current tuning, the tuning range was limited by the carrier loss to 275 GHz, at which point the isolation had

degraded to <10 dB. This again underscores the need for a design that is more robust to waveguide loss.

The integrated filter and coupler Add-Drop Multiplexers suffered from the same high fiber-to-fiber loss. The filter effect was demonstrated qualitatively, whereas the coupler did not perform as designed with only 65% coupled to the 'cross' waveguide. The most likely cause of this problem is poor process control with respect to the waveguide separation and width.

In conclusion, the results from the filter, combined with modeled results from higher-order filters demonstrate both the potential and the limitations of this device structure. It is possible to design and fabricate filters with very narrow bandwidth (<20GHz), with several channels spacing of tuning range through current injection. However, although the isolation and bandwidth of these filters show little sensitivity to waveguide losses, the insertion loss is high and increases rapidly with increased waveguide loss from tuning current. For most practical applications, amplification is probably necessary to overcome this limitation.

5.2 Suggestions for future work

The purpose of this section is to point to a number of potential improvements or extensions to the device structure covered in this dissertation. The first part will discuss changes to improve on the existing structure and functionality. The second part will then focus on additions and extensions of the existing designs for added functionality.

The first step is clearly implementation of the higher-order filters that were designed in Chapter 2. As the theory pointed out — confirmed by subsequent measurements — the first-order filters are simply incapable of meeting the performance requirements of virtually any real application. The main problem, waveguide propagation loss, has much less impact on the fifth-order filters. In addition to this, even for small values of loss or completely without loss, the performance is clearly superior.

The second obvious area in need of improvement is the coupling from fiber to chip. Appropriate lensed fibers in conjunction with integrated mode-converters on the chip have the potential of vastly improving the coupling efficiency. Further reduction in fiber-to-fiber loss can be achieved by monolithic integration of semiconductor optical amplifiers on the same chip as the filters or ADMs. The InP platform and device architecture lends itself very well to this integration.

Finally, in this work switching speed was given marginal consideration. With carrier injection as the tuning mechanism, the inherent limit to switching time is in the ns-range, but to achieve this, more attention must be paid to the additional details of the device design. In particular, the contacts should be designed for low capacitance, and the series resistance reduced, in order to achieve electrical RC-bandwidth in the GHz-range.

With this we turn to enhancements of the existing designs for devices with more functionality.

An important limitation with the λ/4-shifted filters, both first-order and higher-order filters, is the capability to handle many channels over a wide wavelength span. This limitation, posed by the stopband bandwidth of the DBR grating, is in the range of 600-1200 GHz. For applications in systems with wider bandwidth, this range can be extended by a two-stage approach, illustrated in Figure 5.1.

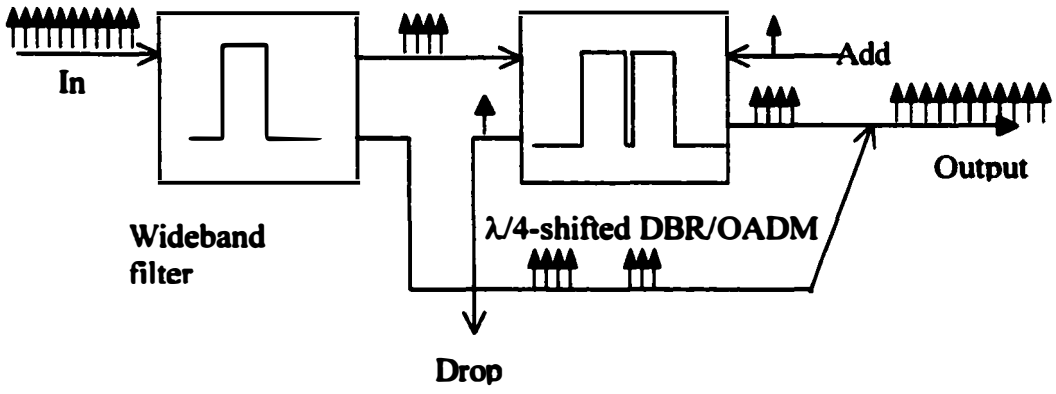

Figure 5.1. *Wide-band, two-stage add-drop multiplexer. The arrows symbolize the wavelength channel spectrum.*

Here the first stage is a wide bandwidth filter, e.g. an add-drop filter based on a single, apodized DBR filter. This multiplexer picks out a group of channels with a total wavelength span compatible with the capability of the narrowband ADM based on the λ/4-shifted DBR filters described in this work. The main requirements to this first-stage filter are steep filter skirt, side-lobe suppression and low cross-talk. The narrow-band ADM then performs the add-drop operation on one channel, before the entire group of wavelengths is recombined with the channels that bypassed the second stage filter. This approach removes the

limitations on maximum bandwidth, at the expense of chip size and complexity. The stopband of the first stage must be narrower than that of the second stage, and it is necessary to use an apodized grating for the first filter, to suppress cross-talk due to side-lobes.

The last proposed enhancement illustrates the potential for integration on a semiconductor platform. As already discussed above, the architecture and platform is suitable for integration with active devices, such as amplifiers, lasers and waveguide detectors. Figure 5.2 shows an example of this. The suggested device consists of an add-drop multiplexer, with a modulated laser source on the add-port and a detector on the drop port. This forms an integrated module with two fiber ports and two electrical ports, a one-chip channel-dropping network interface without the need for external optical components or active devices. A simpler version can be based on a filter, without the directional coupler, integrated with a detector, for a wavelength selective receiver module.

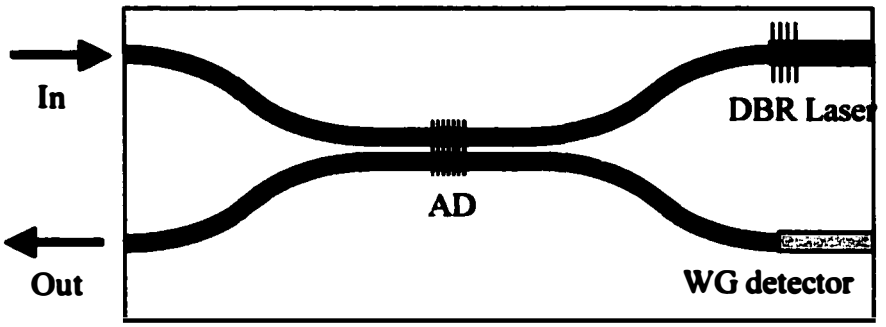

Figure 5.2. *Integrated add-drop network access chip with an add-drop multiplexer for channel selection, a waveguide receiver detector and a modulated DBR laser transmitter*

The examples given in this section highlights some of the potential for increased functionality of a semiconductor-based add-drop multiplexer.

Compared to fiber or SiO_2-on-Si based multiplexers, the semiconductor devices lend themselves very well to integration. In addition to this, the ability to tune by injection of carriers gives the potential for very short switching time, compatible with true packet switching in dynamically reconfigurable networks. At the same time, it is clear that ADMs based on DBR gratings in semiconductor can not rival the SiO_2-Si arrayed waveguide gratings in terms of channel count, channel spacing or static filter performance. This means that the SiO_2-Si based devices are more suitable for applications where fast switching is not required, but the static performance is important. However, the semiconductor-based ADMs are potentially very competitive in applications where fast switching, small size, or integration with active components is essential. Most notably in packet-switched optical networks, where presently no other alternative exists for all-optical switching at packet rates.

Appendix A

Add-Drop Multiplexer device fabrication

Add-Drop Multiplexer Device Process

1. Grating pattern

Remove InP cap layer:

HF:DI (3:1)

Deposit SiN mask

PECVD, 300 Å

Photolithography:

Spin AZ 4110, 4k, 30 secs

Bake 95° hotplate, 1'

Mask expose, 8"

Develop ~50"

Hardbake, 10' @ 120°C oven

Descum

20", plasma etcher, 100W, 300 mTorr

Etch SiN:

RIE : $SF_6/O_2/Ar$: 5/3/10 sccm

20 mTorr, 250 V

Etch time : 1'

Remove polymer

Remove PR (Acetone)

2. Grating process

Solvent Clean

Boiling Acetone (> 3mins)

Isopropanol

Rinse Iso, on spinner

Nitrogen dry, on spinner

Spin HMDS

6k rpm, 1 min.

Spin Photoresist

Shipley 1400-5a

6k rpm, 1'

Bake on hotplate : 95°C – 1 minute

Holographic Exposure

30nA·min (Power reading should be ~40nA photocurrent)

Develop

AZ400k:DI (1:4), 12 secs.

Bake 120°C/ 10 min (oven)

Descum O_2 plasma

300W, 100mT, 5 secs

Grating dry etch process:

Chamber pre-clean:

20 sccm O_2, 500V, 125 mT , 20 mins

Chamber pre-coat:

20/4/10 sccm MHA, 500 V, 75 mT, 10 mins

Load sample

Sample coat:

20/4/10 sccm MHA, 200 V, 125 mT, 2 mins

Etch:

20/4/10 sccm MHA, 500 V, 75 mT (etch rate of InP ~ 700 Å/min)

Polymer removal:

20 sccm O_2, 300 V, 125 mT, 1'30"

Remove photoresist w. Acetone

Remove SiN in HF

Prepare sample for regrowth

Solvent clean (Acetone, Isopropanol)

O_2 –plasma, 300 mT, 100 W, 3 minutes

UV-ozone, 30 minutes

HF dip (immediately before loading sample in MOCVD reactor)

3. Regrowth

0.3μm uid InP

1.5μm p-InP (7e17)

0.15μ p+-InGaAs contact layer (2e19)

4. Ridge process

Deposit SiN mask for waveguide definition

Solvent clean

PECVD : 3000Å SiN_x

Photolithography (waveguide pattern):

Stepper :

Spin SPR-510 , 4k, 30"

Bake, 90°C, 3'

Expose (Stepper), 1.2" (mask layer GDS-4)

Develop : Undiluted MF701, 40-45"

Contact aligner:

Spin AZ 4110, 4k, 30 secs

Bake 95° hotplate, 1'

Mask expose, 8"

Develop ~50"

Hardbake, 10' @ 120°C oven

Descum

20", plasma etcher, 100W, 300 mTorr

Etch SiN:

RIE : $SF_6/O_2/Ar$: 5/3/10 sccm

20 mTorr, 250 V

Etch time : 2'30"

Remove polymer

Remove PR (Acetone)

Etch waveguide:

RIE#2 : MHA 4/20/10

Standard process (see grating etch section for conditions)

Etch time : 10' (Etch depth should be 6500 ~Å)

Polymer removal : 5'

Photolithography

As above – (mask layer GDS-5)

Descum

20", 100 W, 300 mTorr

Etch SiN:

As above

Etch waveguide and isolation trenches:

Etch time : 8'30" (Etch depth WG : 13,500 Å , isolation : 5,300 Å)

Polymer removal : 4'

Remove SiN

HF:DI dip

5. Planarization process

Planarization:

Spin SF15, 5k, 30"

Dektak

Reflow : 250°C Hotplate, 2'

Dektak

(Repeat until sample is planar – typically 3 layers)

Deep UV exposure : 2'

Develop in SAL 101, 10" steps until ridges are clear

(watch for interference fringes)

Repeat exposure if develop stops or slows significantly.

6. p-metal contact

Photolithography

Lift-off process

Evaporate p-contacts:

Ti/Pt/Au : 250Å/300Å/6000Å

Lift-off

7. Pattern PMGI for cleaving

Pattern SF15:

Deep UV expose : 2'

Develop undiluted SAL 101

Repeat until clean

Anneal p-contact

420°C, 15" (standard recipe)

8. Backside process

Thin substrate to ~100μm thickness

Backside metal

E-beam deposition of Ni/AuGe/Ni/Au : 100/1000/200/1500 Å

Anneal 20 secs @ 380°C